

NOAA Technical Memorandum ERL NSSL-81

MESOCYCLONE EVOLUTION AND TORNADO GENERATION  
WITHIN THE HARRAH, OKLAHOMA STORM

Edward A. Brandes

Property of  
NWC Library  
*University of Oklahoma*

National Severe Storms Laboratory  
Norman, Oklahoma  
May 1977

UNITED STATES  
DEPARTMENT OF COMMERCE  
Juanita M. Kreps, Secretary

NATIONAL OCEANIC AND  
ATMOSPHERIC ADMINISTRATION  
Robert M. White, Administrator

Environmental Research  
Laboratories  
Wilmot N. Hess, Director



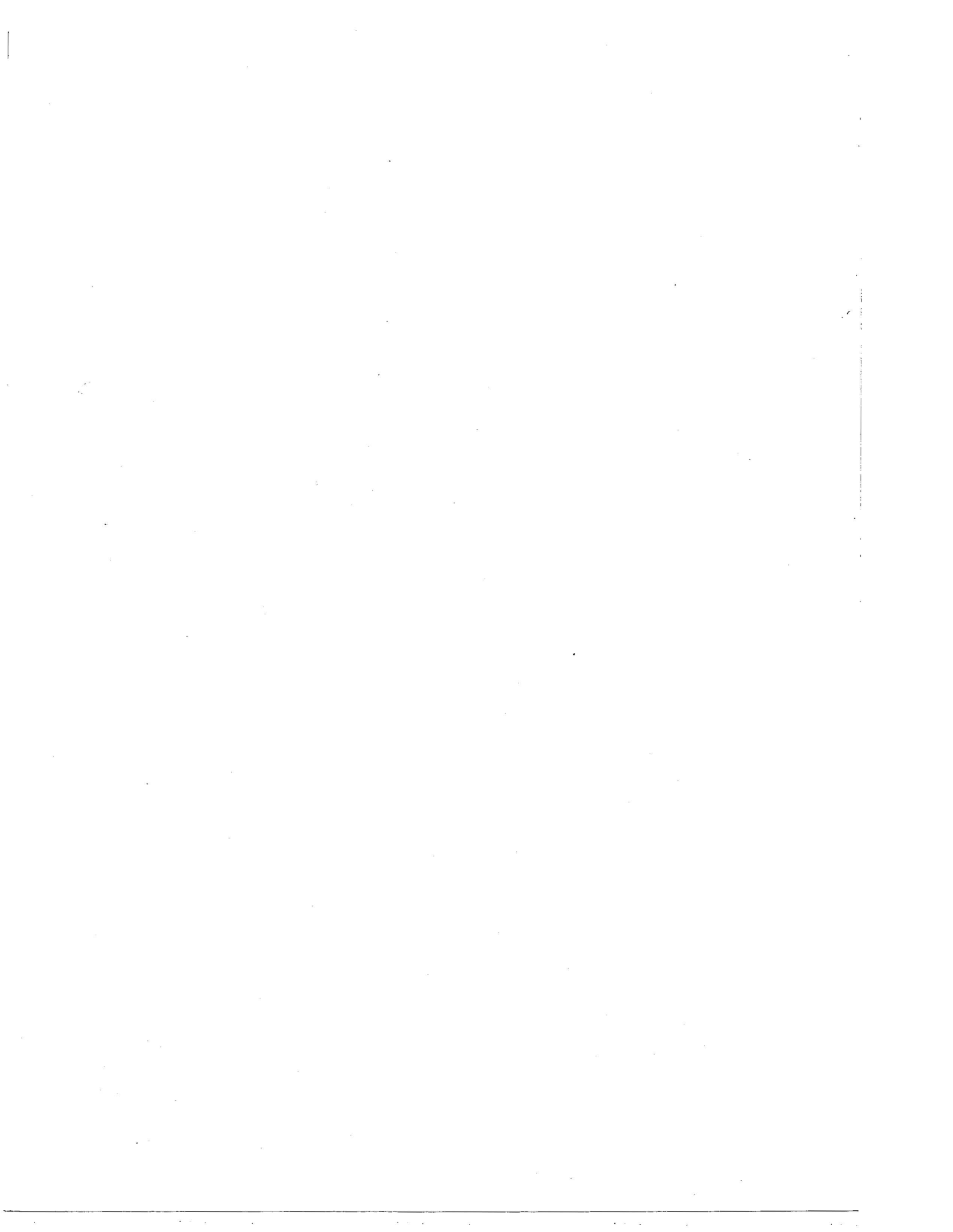


## TABLE OF CONTENTS

	<u>Page</u>
LIST OF FIGURES	.iv
ABSTRACT	1
1. INTRODUCTION	1
2. DATA AND ANALYSIS	2
3. OBSERVATIONS	3
3.1 1515 CST: Early Mesocyclone Flow Structure	3
3.2 1530 CST: Mesocyclone Intensification	8
3.3 1543 CST: Formation of the Incipient Tornado Vortex	9
3.4 1553 CST: Damaging Tornado on the Ground	9
3.5 1603 CST: Tornado Dissipation	16
3.6 Subsequent Observations	17
3.7 Summary	17
4. FORMATION OF INTENSE VORTICES	23
5. CONCLUSION	26
6. ACKNOWLEDGMENTS	26
7. REFERENCES	26

## LIST OF FIGURES

<u>Figure</u>		<u>Page</u>
1	Contoured PPI displays ( $0^\circ$ antenna elevation) for 8 June 1974: a) WSR-57 range normalized display (40 km range marks) showing first echo location, Harrah storm, and b) - d) Doppler display (20 km range marks, not range normalized) giving subsequent storm development.	4
2	Stüve diagrams for environmental soundings released at Norman, Oklahoma on 8 June 1974. Wind scale ( $\text{m s}^{-1}$ ) is at lower right and balloon ascent (MSL height versus time) shown by a series of circles.	5
3	Horizontal perturbation wind fields (with Cimarron radar reflectivity in dBZ superimposed) and vertical velocity patterns ( $\text{m s}^{-1}$ ) at 1515 CST. Circles denote velocities $< 0.5 \text{ m s}^{-1}$ , north is toward the top of the figure, and heights are AGL. Level mean flow vectors (removed) are also given.	6
4	Radial-height distributions of mean tangential ( $v_t$ ), radial ( $v_r$ ), and vertical ( $w$ ) wind during early mesocyclone development (1515 CST). Positive velocities ( $\text{m s}^{-1}$ ) designate cyclonic, outward, and upward motion.	7
5	Horizontal wind fields, as in Fig. 3, showing mesocyclone intensification (1530 CST). Major surface wind discontinuities and anomalous shear zones $\geq 2 \times 10^{-2} \text{ s}^{-1}$ (indicated with ●) added.	10
6	Radial-height velocity distributions, as in Fig. 4, showing mesocyclone intensification (1530 CST).	11
7	Horizontal wind fields, as in Fig. 5, during appearance of incipient tornado vortex (1543 CST). Tornado damage path shown by stippling.	12
8	Radial-height velocity distributions, as in Fig. 4, during appearance of incipient tornado vortex (1543 CST).	13

<u>Figure</u>		<u>Page</u>
9	Horizontal wind fields, as in Fig. 7, while damaging tornado is on the ground (1553 CST).	14
10	Radial-height velocity distributions, as in Fig. 4, while tornado is on the ground (1553 CST).	15
11	Horizontal wind fields, as in Fig. 7, following tornado dissipation (1603 CST).	18
12	Radial-height velocity distributions, as in Fig. 4, following tornado dissipation (1603 CST).	19
13	Horizontal wind fields, as in Fig. 7, showing continued mesocyclone decline (1611 CST).	20
14	Radial-height velocity distributions, as in Fig. 4, showing continued mesocyclone decline (1611 CST).	21
15	Mesocyclone azimuth averaged vertical profiles of radial wind, tangential wind, inflow angle, and mean horizontal angular momentum flux at 3.6 km radius.	22



# MESOCYCLONE EVOLUTION AND TORNADO GENERATION WITHIN THE HARRAH, OKLAHOMA STORM

Edward A. Brandes

The updraft mesocyclone of a tornado producing thunderstorm on 8 June 1974 was first detected aloft along a convergent and cyclonically sheared boundary between inflow air entering forward and rear storm quadrants. Maximum tangential flow was contained in a jet-like annulus averaging less than 4 km in radius (depending upon the development stage) that lowered to ground prior to tornado genesis. Although mesocyclone inflow was within a variable surface layer 3 to 6 km deep, it concentrated between 1 and 3 km elevation. During the tornadic phase maximum mass flux and angular momentum transport were observed, and the parent mesovortex exhibited features associated with breakdown, i.e., a transition from single-cell to two-cell axial flow structure with an enlarged core radius above the stagnation point. During breakdown several small eddies appeared along an elongated horizontal axis.

The tornado originated similarly aloft (between 1 and 5 km elevation) on the mesocyclone's principal vertical axis. The tornado dissipated when cyclonic rotation of the elongated horizontal axis choked the supply of inflow air and detached the tornado from the principal updraft.

## 1. INTRODUCTION

On 8 June 1974 an outbreak of more than 20 tornadoes killed 17 persons and injured hundreds in central and northeastern Oklahoma. Many storms developed within the National Severe Storms Laboratory (NSSL) dual-Doppler area and were sampled repeatedly during their lifetimes. In a preview (Brandes, 1976) measurements of two storms were used to describe a consistent basic mesocyclone-evolution pattern and a specific wind-flow configuration that existed at ground levels during tornado genesis. This study addresses tornado formation by examining mesocyclone life cycle and kinematic properties in one storm that produced a tornado near Harrah, Oklahoma. Results are generalized via similarities observed in other storms and by comparison with Ward's (1972) laboratory vortex model. Vorticity generation and distribution in the Harrah storm are discussed by Heymsfield (1976) and Ray (1976).

Here tornadoes are essentially a subgrid phenomenon whose properties must be inferred from raw (unsmoothed) Doppler radar measurements. A proposed model for tornado genesis applies to squall line storms where the parent vortex (mesocyclone) elongates and may produce either a single tornado or tornado families in parallel modes, i.e., the damage path is interrupted and consists of parallel segments (Fujita, 1974; Agee *et al.*, 1976). Interactions with coexisting storm cells or the thunderstorm environment are not considered. Storm wind patterns are displayed in both horizontal cross-sections and as radial-height distributions of mean radial, tangential, and vertical flows.

## 2. DATA AND ANALYSIS<sup>1</sup>

The data consist of coordinated volumetric sampling sequences from 2 S-band Doppler radars approximately 40 km apart at Norman and Oklahoma City (Cimarron Field), Oklahoma. Individual radar measurements usually were spaced 1° in azimuth, 1° in elevation, and 0.6 km in radial range. Details on data acquisition and signal processing are given by Ray *et al.* (1975) and Sirmans and Bumgarner (1975). Procedures used to compute Cartesian wind components and a technical description of the radars can be found in Brandes (1977).

Analyzed products include the horizontal perturbation wind (level mean flow removed), vertical velocity, horizontal divergence, and vertical vorticity fields. Analyzed data planes begin at 0.3 km with 0.5 km vertical separation. For illustration, data are presented only at 0.3, 1.3, 2.8, and 4.8 or 5.8 km elevation. To reduce uncertainties in vertical wind estimates, due to errors inherent in the numerical solution employed here, this component was smoothed by a single application of a nine point filter. The perturbation wind presentation was chosen to aid detection of eddy motion.

At each level, radial ( $v_r$ ) and tangential ( $v_t$ ) wind components (with respect to the mesocyclone center) and vertical velocities ( $w$ ) were averaged over concentric rings (0.8 km in width) centered on the mesocyclone vertical axis. Mean values assigned at ring mid points (i.e.,  $r = 0.4, 1.2, 2.0 \dots 10.0$  km) are presented as radial-height sections. Placement of the mesocyclone axis is subjective but attempts to preserve height continuity. The small number of grid points available for averaging introduces some uncertainty near the rotation axis and asymmetries, which may be

---

<sup>1</sup>All times are Central Standard Time, all heights, AGL. For MSL add 0.37 km.

important in tornado genesis, are lost in the analysis. Nevertheless, the profiles permit a summary of basic mesocyclone kinematic properties not readily apparent in the horizontal cross-sections.

### 3. OBSERVATIONS

The Harrah storm "first echo" appeared at 1406 on the southern end of a north-south squall line (Fig. 1a) that developed east of a dryline and west of a tropospheric wind jet. A small reflectivity appendage (Fig. 1b) and a lowered cloud base became visible on the storm's right rear (south-western) flank about 1505. Dual-Doppler radar sampling commenced 10 min later.

Environmental temperature, moisture, and wind stratification a) east of the squall line, b) just ahead of the thunderstorms, c) behind the squall line, and d) behind the dryline are shown in Fig. 2. Inspection shows a deepening surface moisture layer but little change in thermal structure as the squall line approaches. Also, significant background convergence exists across the thunderstorm line (compare Figs. 2a and 2c) and on forward storm flanks wind speeds increase (Fig. 2b). In the cloud bearing layer, the mean ambient wind was from  $225^\circ$  at  $27 \text{ m s}^{-1}$  and the average storm motion during the severe stage was from  $230^\circ$  at  $13 \text{ m s}^{-1}$ . Although the direction of movement did not vary, the storm decelerated noticeably between the formative and mature stages ( $19$  versus  $12 \text{ m s}^{-1}$ ).

#### 3.1 1515 CST: Early Mesocyclone Flow Structure

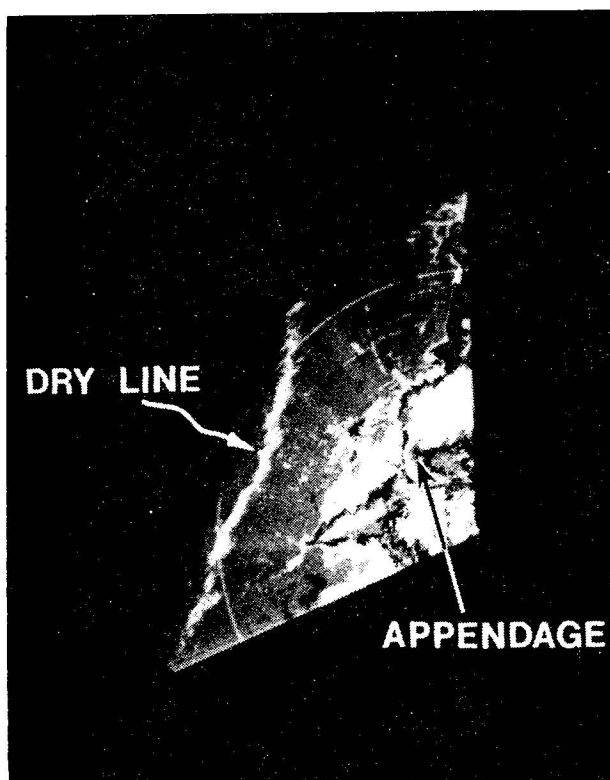
With the storm reflectivity structure already well developed, near peak values were recorded at 1515; but updraft rotation was only in the nascent stage. Note the convergent and cyclonically curved flow at 0.3 km (Fig. 3) on the southwestern storm flank.<sup>2</sup> Radial velocities (with respect to the mesocyclone center, Fig. 4) exceed swirl (tangential) components near ground with maximum inflow and maximum moisture flux (deduced with Fig. 2) concentrated at approximately 2 km elevation. The average depth of the inflow layer ( $\bar{h}$ ) is about 4.5 km. Aloft, peak tangential winds encircle

---

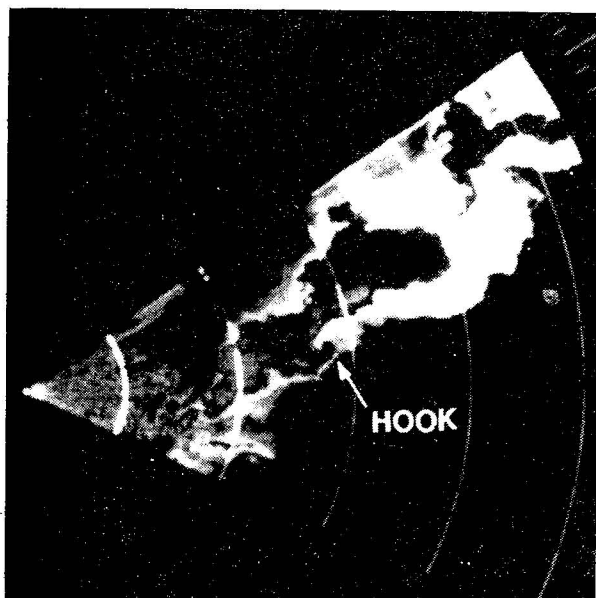
<sup>2</sup>Incomplete data sampling and proximity to the base line between radars ( $310^\circ$  azimuth from the Norman radar) truncate substantially the storm flow pattern. In the base line vicinity, both radars see essentially the same wind component and spurious three-dimensional wind estimates arise (see, upper elevations in Fig. 3). Hence, averaged data beyond 4 km radius and at upper levels in Fig. 4 are suspect.



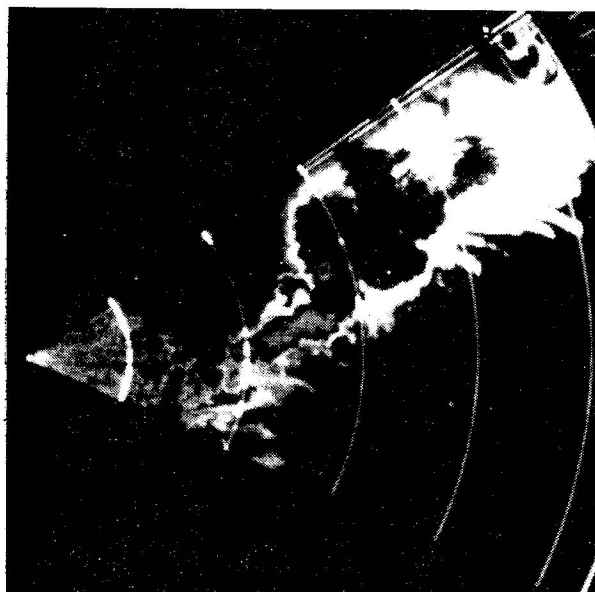
a. NSSL WSR-57, 1406 CST.



b. Norman Doppler, 1505 CST.

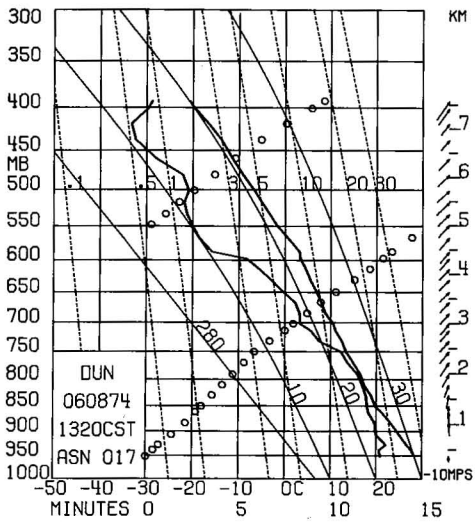


c. Cimarron Doppler, 1548 CST.

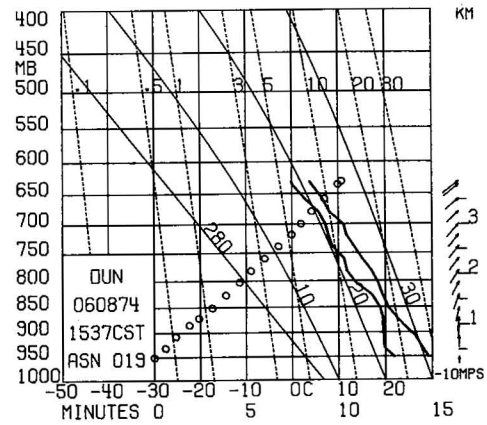


d. Cimarron Doppler, 1608 CST.

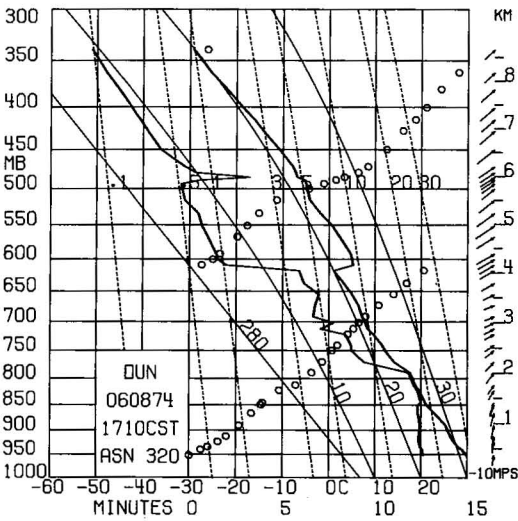
Figure 1. Contoured PPI displays ( $0^\circ$  antenna elevation) for 8 June 1974: a) WSR-57 range normalized display (40 km range marks) showing first echo location, Harrah storm, and b) - d) Doppler display (20 km range marks, not range normalized) giving subsequent storm development.



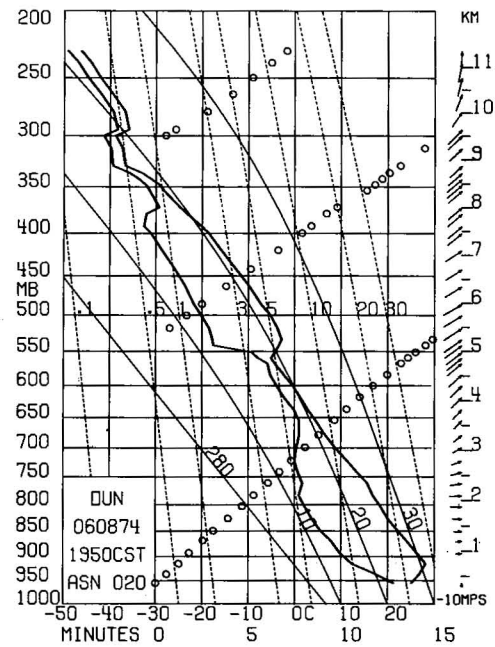
a.



b.



c.



d.

Figure 2. Stüve diagrams for environmental soundings released at Norman, Oklahoma on 8 June 1974. Wind scale ( $m s^{-1}$ ) is at lower right and balloon ascent (MSL height versus time) shown by a series of circles.

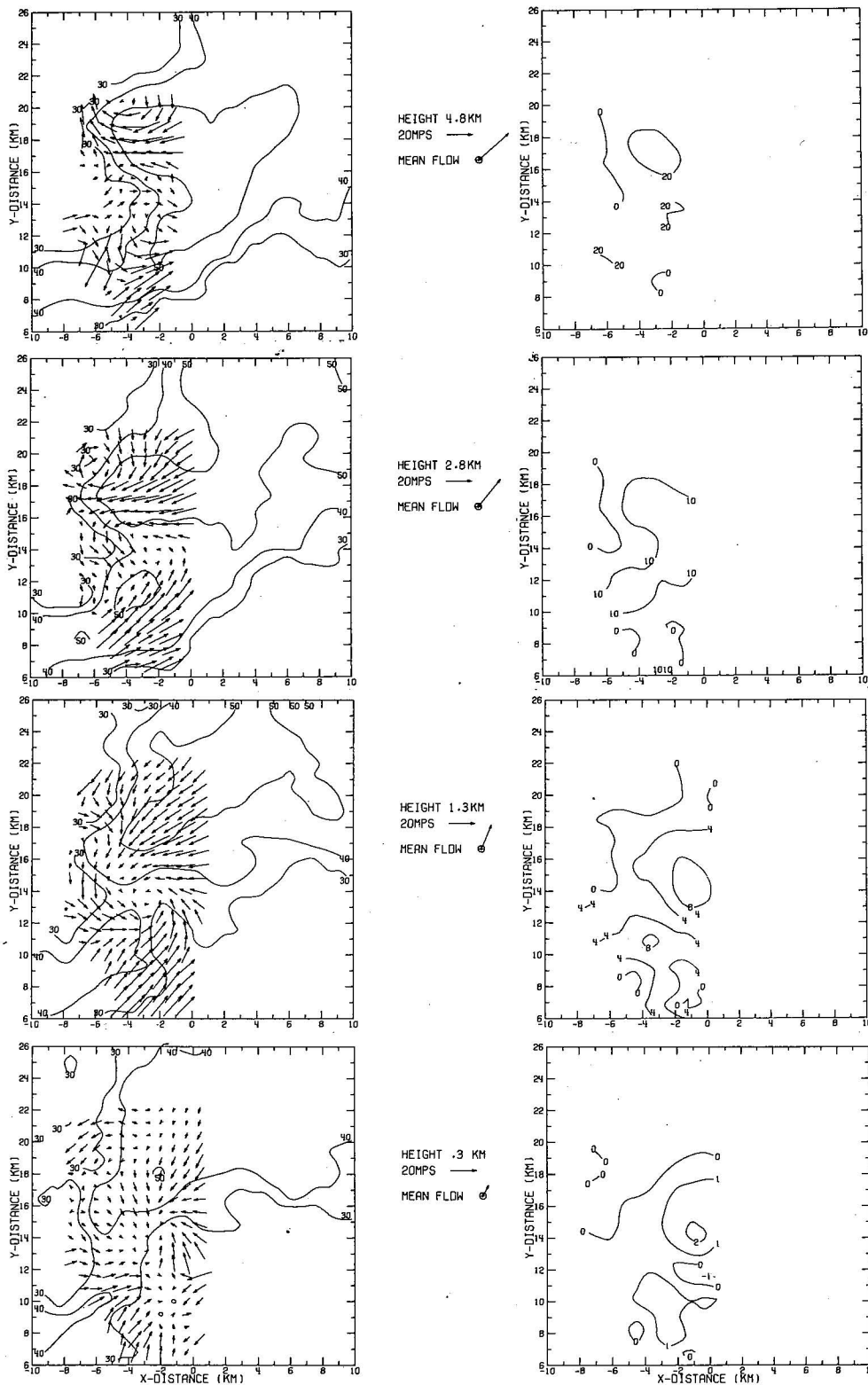


Figure 3. Horizontal perturbation wind fields (with Cimarron radar reflectivity in dBZ superimposed) and vertical velocity patterns ( $m s^{-1}$ ) at 1515 CST. Circles denote velocities  $< 0.5 m s^{-1}$ , north is toward the figure top and heights are AGL. Level mean flow vectors (removed) are also given.

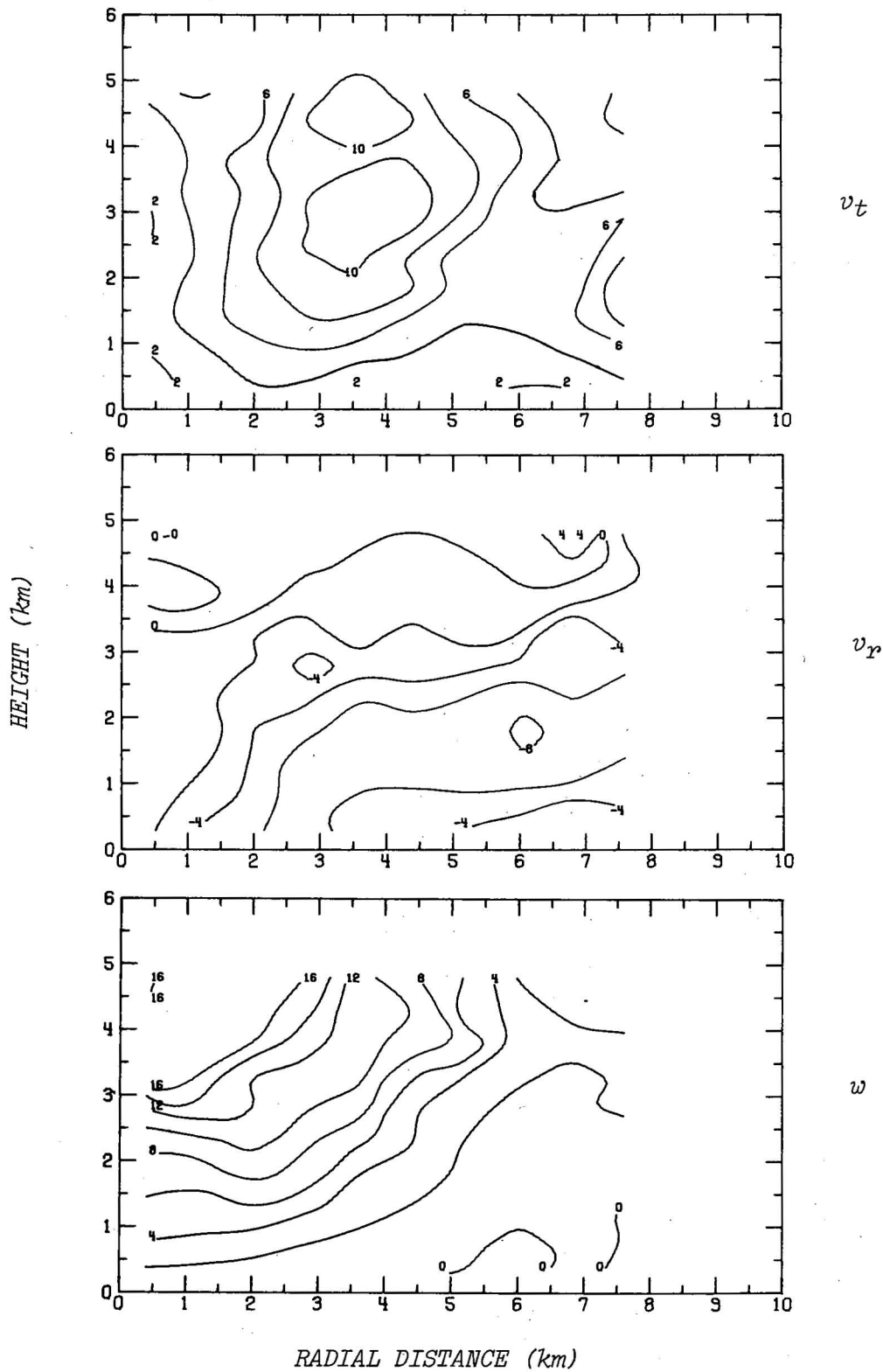


Figure 4. Radial-height distributions of mean tangential ( $v_t$ ), radial ( $v_r$ ), and vertical ( $w$ ) wind during early mesocyclone development (1515 CST). Positive velocities ( $\text{m s}^{-1}$ ), designate cyclonic, outward, and upward motion.

an interior portion of the mesocyclone (the core) in an annulus of 3.5 km mean radius ( $\bar{r}_C$ ). Averaged axial (vertical) flow increases linearly with height and decreases from the vertical axis. Weak downdrafts reside on the western storm flank and beneath high reflectivity portions.

The mesocyclonic vortex, most pronounced between 2 and 3 km elevation, is elliptically shaped. Updrafts reach a maximum near the vertical axis and in a convergent zone of high speed horizontal flow between the mesocyclone center and an anticyclonic feature on the storm's northwestern flank. Typically, anticyclonic eddies form only at higher elevations near horizontal wind maxima; exhibit little net vertical motion; and are far more transient than their cyclonic counterparts.

South of the mesocyclone (see  $z = 2.8$  km) a second convergent zone exists between southwest and northwest flow. Later, as a sharp gust front separating storm outflow from inflow, this boundary descends to ground levels.

### 3.2 1530 CST: Mesocyclone Intensification

Between 1515 and 1530 a vigorous surface gust front developed southward from the mesocyclone (Fig. 5) and above 1 km a new convergent area or bulge in the mesocyclone extended toward the northwest. More evident now is the cyclonic shear and convergence between air entering forward (eastern) and rear (western) storm quadrants. Inflow, primarily from forward flanks, converges cyclonically to produce a broad horizontal wind maximum behind the wind core bulge.

Mesocyclone meridional (radial) flow increased for radial distances less than 2 km but apparently weakened (temporarily) at larger radii (Fig. 6). Tangential flow intensified throughout the storm depth considered here. Strongest vertical winds are located where the tangential wind core intersects the gust front near ground and close to the mesocyclone center above 3 km. Not only did the principal updraft intensify but also it narrowed in width.

A weak echo region (WER, Marwitz, 1972) is evident within the mesocyclone core near the principal updraft. Fairly common in severe storms, the WER long has been recognized as an updraft signature (Browning, 1964). At higher elevations, the updraft and circulation center become the locale of both maximum radar reflectivity and highest echo tops. Between 1.5 and 3.0 km elevation, a distinct shear region ( $2.0 \times 10^{-2} \text{ s}^{-1}$ , indicated with ●) and possible tornado-scale vortex was detected in raw velocity measurements within the northwestward protruding wind disturbance. Similar shear anomalies, with horizontal dimensions of ~1 km (the azimuthal distance between two adjacent Doppler measurements), correspond to tornadoes in other storms (Burgess *et al.*, 1975). Embedded within the larger cyclonic circulation, this shear anomaly is the first indication of multiple vortices within the Harrah storm mesocyclone. A branch of the main updraft extends to the anomaly and a small weak downdraft is located to the south.

### 3.3 1543 CST: Formation of the Incipient Tornado Vortex<sup>3</sup>

Several notable changes in mesocyclone structure took place prior to tornado touchdown. Tangential and meridional flows below 3 km intensify and combine to greatly increase angular momentum transport and vorticity production (Figs. 7 and 8). Two local shear anomalies, extending from 1 to 5 km elevation, are now present in the unsmoothed Doppler measurements. One anomaly ( $2 \times 10^{-2} \text{ s}^{-1}$ ) is situated at the mesocyclone center and is thought to be the embryonic tornado circulation, while the other averages  $3 \times 10^{-2} \text{ s}^{-1}$  and resides within the wind core bulge. Clearly, the southern boundary of a region of strengthening and southward turning wind, this protuberance had rotated slightly counter-clockwise (see  $z = 2.8 \text{ km}$ ).

The main storm updraft, collocated with the mesocyclone vertical axis previously, now slopes northwestward with height and continues to strengthen. Collapse of the WER is manifest by the increase in high reflectivity areal coverage at all elevations -- more so within the mesocyclone core. Downdrafts have strengthened slightly and cover increasingly larger areas north through east. A prominent hook echo first was detected after the 1543 data collection sequence (Fig. 1c). The apparent correlation between downdraft and mesocyclone flow intensification with hook echo development was noted in another study (Brandes, 1977).

### 3.4 1553 CST: Damaging Tornado on the Ground

Proximity of the 1543 circulation center to the surveyed damage path suggests the tornado touched ground shortly afterwards. Tornado genesis, along the major horizontal axis (at a focal point of the now elliptical surface mesocyclone), is in a region compressed by strong convergent flow and across which high shears exist (Fig. 9). The distinctive shear anomaly coinciding with the tornado approaches  $5 \times 10^{-2} \text{ s}^{-1}$  in the unsmoothed Doppler measurements and extends vertically from ground to strong divergent flow at 5 km. The small discrepancy between the radar indicated tornado location and the damage path is attributed to either data processing or possible radar orientation error.

The resultant surface wind configuration with a "psuedo-cold front" (extending southward) and a diffuse convergent zone or "warm front" (extending northward) recalls synoptic wave cyclone development on the polar front. This pattern has been observed in Doppler derived wind patterns of other storms (e.g., Brandes, 1976) and is similar to that determined from surface wind observations by Lemon (1976) and others. Moreover, the

---

<sup>3</sup>Reflectivity maxima ( $\geq 30 \text{ dBZ}$ ) 10 km southeast of the mesocyclone at this and later periods are chaff released to illuminate the storm's inflow region (McCarthy *et al.*, 1974).

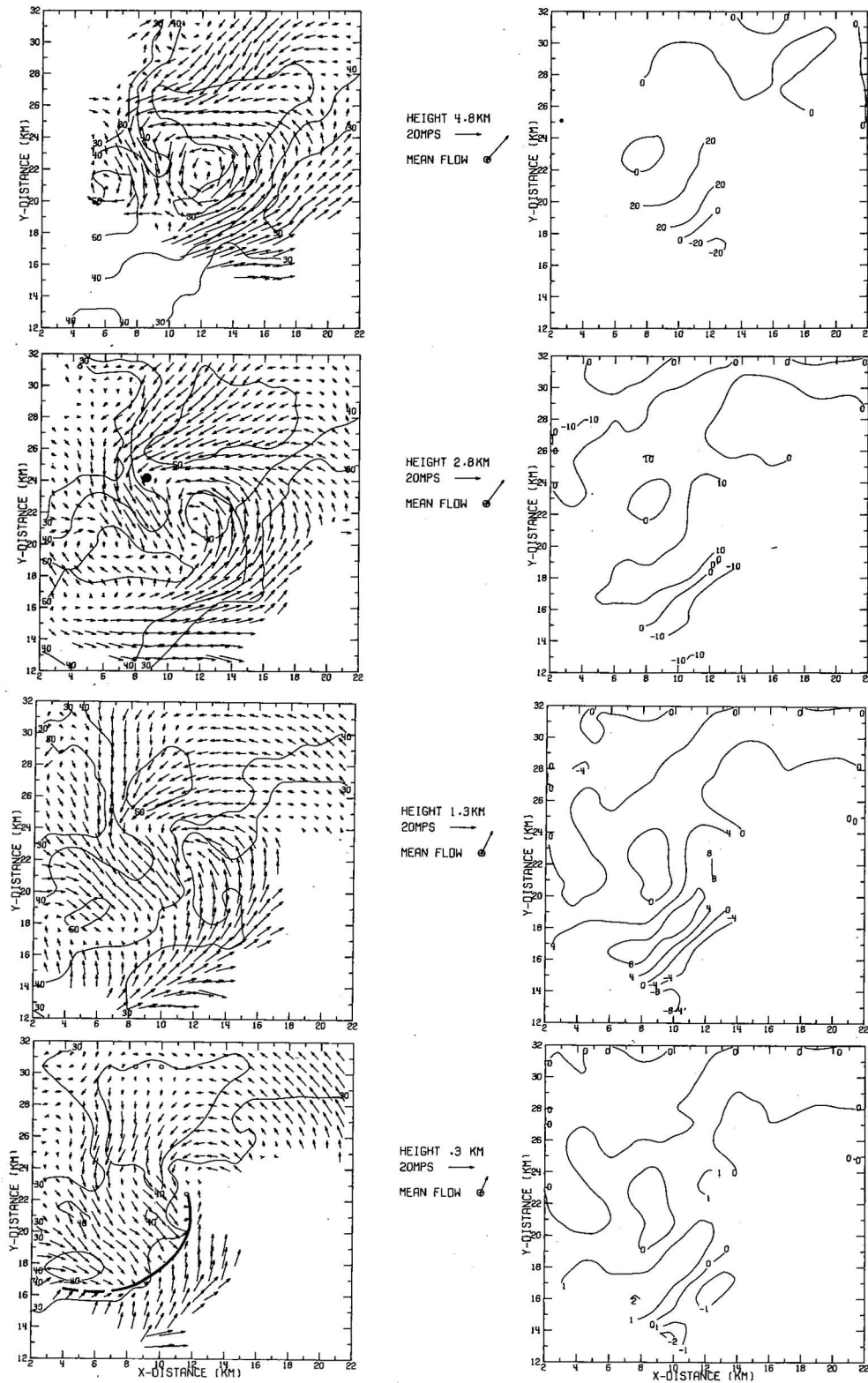


Figure 5. Horizontal wind fields, as in Fig. 3, showing mesocyclone intensification (1530 CST). Major surface wind discontinuities and anomalous shear zones  $\geq 2 \times 10^{-2} \text{ s}^{-1}$  (indicated with ●) added.

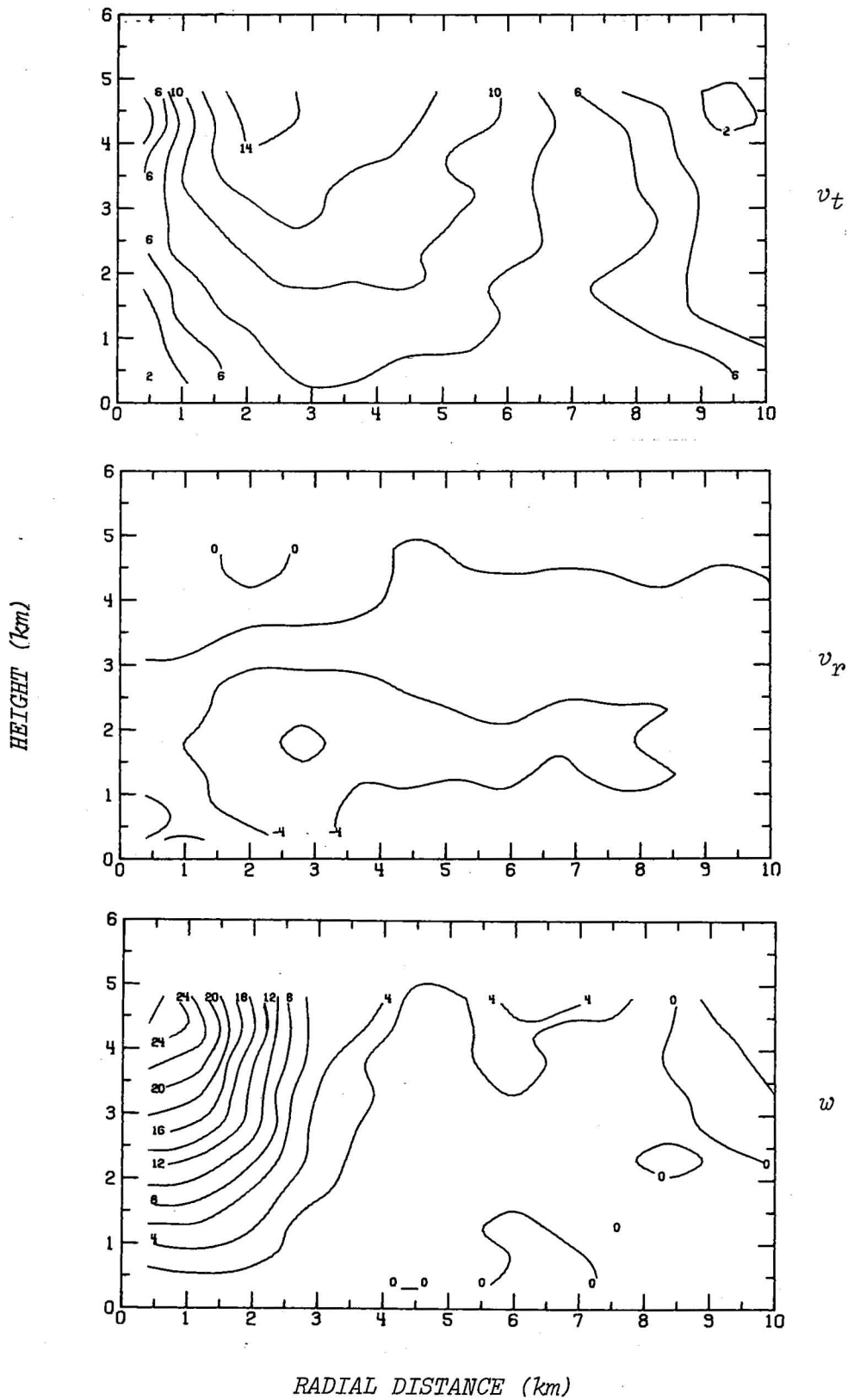


Figure 6. Radial-height velocity distributions, as in Fig. 4, showing mesocyclone intensification (1530 CST).

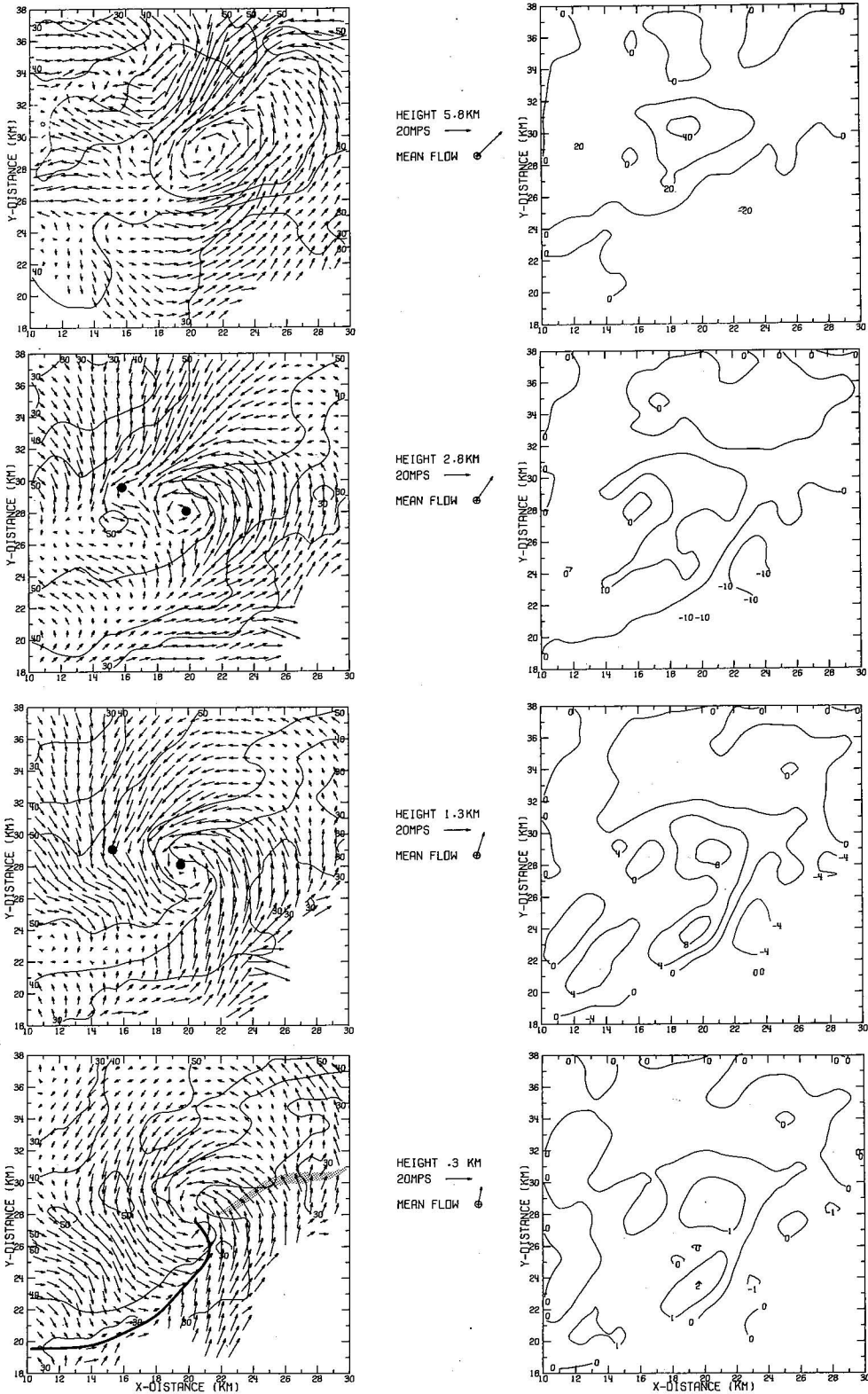


Figure 7. Horizontal wind fields, as in Fig. 5, during appearance of incipient tornado vortex (1543 CST). Tornado damage path shown by stippling.

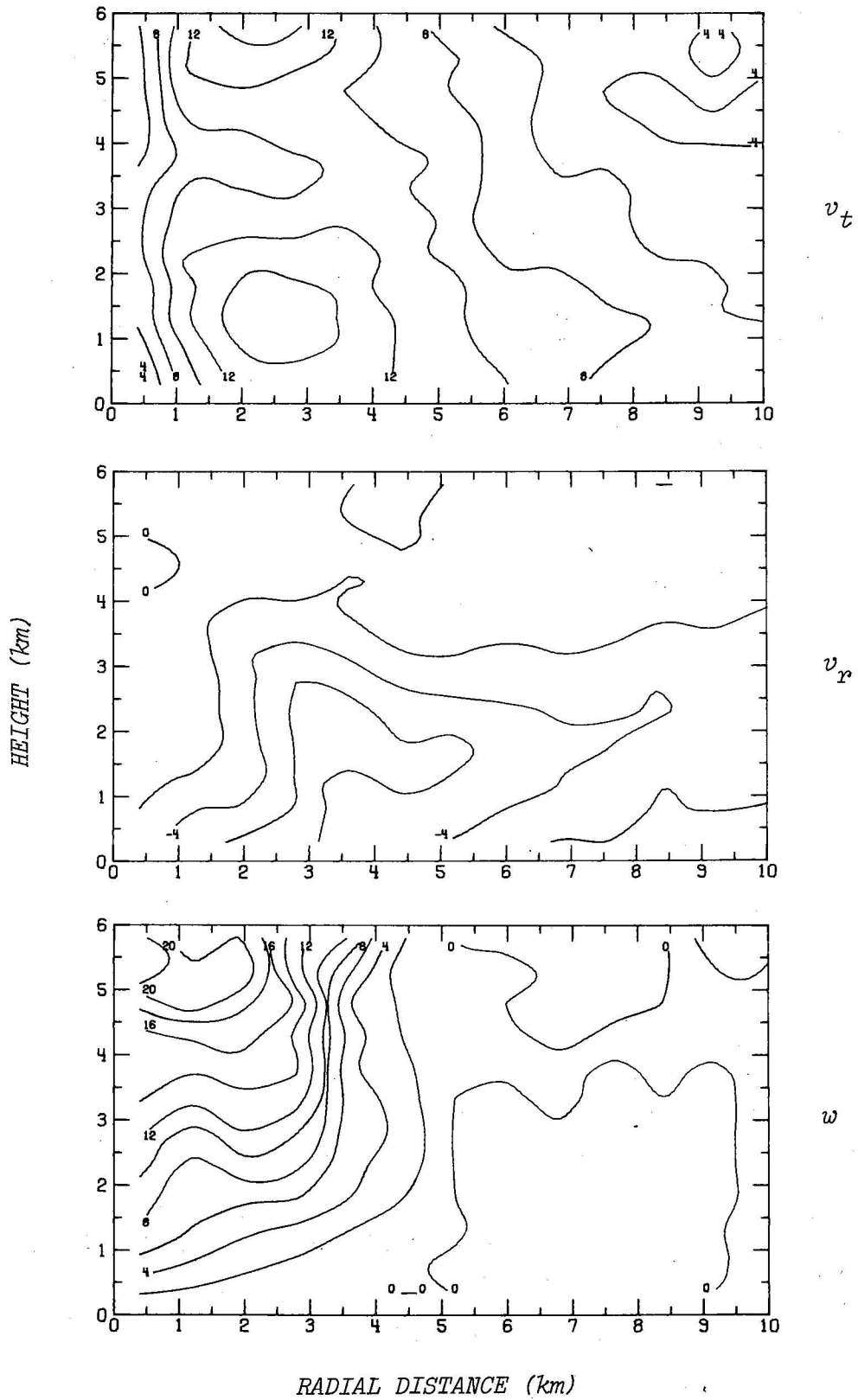


Figure 8. Radial-height velocity distributions, as in Fig. 4, during appearance of incipient tornado vortex (1543 CST).

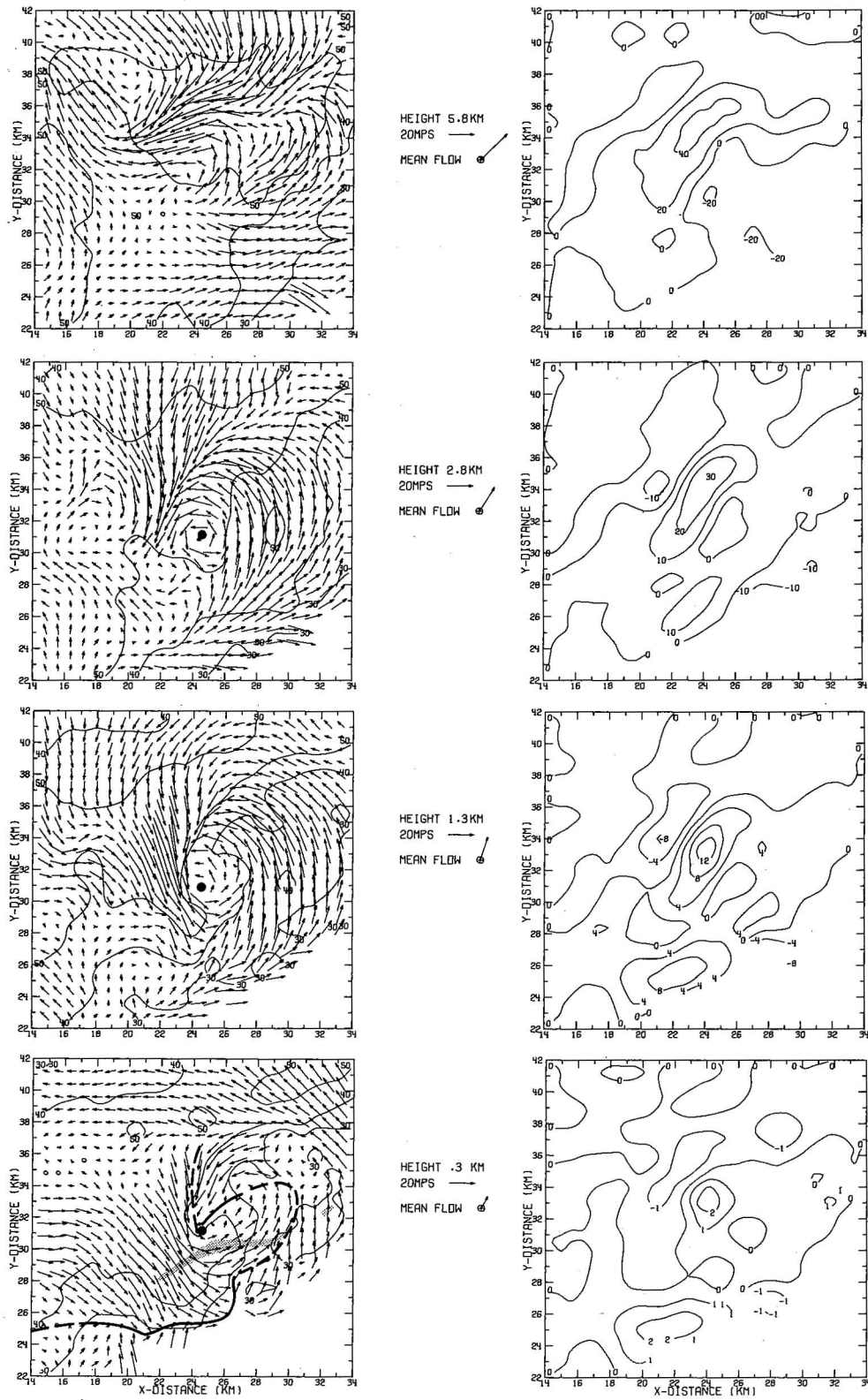


Figure 9. Horizontal wind fields, as in Fig. 7, while damaging tornado is on the ground (1553 CST).

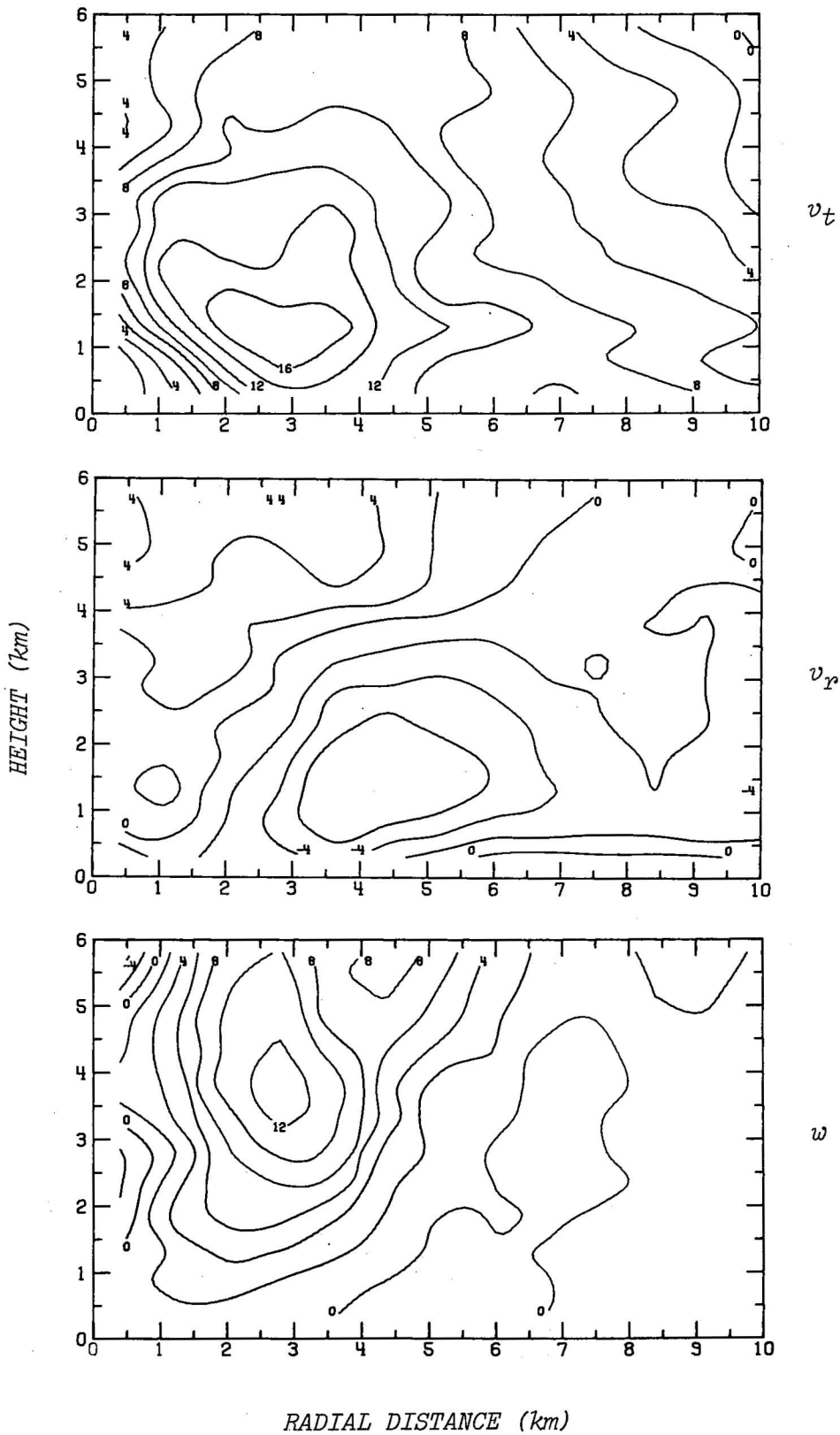


Figure 10. Radial-height velocity distributions, as in Fig. 4, while tornado is on the ground (1553 CST).

elongated mesocyclone axis could be a rolled-up section of the convergent boundary separating air originally entering forward and rear storm quadrants. A second diffuse circulation center can be seen northeast of the tornadic vortex (0.3 km elevation). Agee *et al.* (1976) deduced a multiple vortex configuration within mesocyclones from cloud observations and surveys of tornado damage paths. However, in the Harrah storm at this time, only the tornadic vortex has height continuity.

Moist inflow to the tornadic vortex enters the storm ahead of the gust front and has a long penetration path through regions of moderate radar reflectivity. Mergence with storm outflow creates strong local convergence and cyclonic shear at the mesocyclone core radius near the tornado. Analysis smoothing and raw velocity measurements suggest the distance between the tangential wind band and the enclosed tornado is less than implied by Figs. 9 and 10. The immediate tornado environment is further characterized by light vertical winds and by high horizontal gradients of vertical velocity (computations on a 0.8 km grid). Peak vertical velocities, which increased abruptly during tornado genesis, have been displaced to the mesovortex core wall and are found 2 km farther north. The updraft is flanked by an intense centrally located downdraft on the northwest and by a developing downdraft on the southeast. Almost entirely contained within the enlarged mesovortex core, the second downdraft may signify a transformation from a single-cell to a two-cell axial flow structure and may indicate mesovortex breakdown. When viewed from the east, the tornado was unobstructed suggesting this downdraft at 1553 is relatively precipitation free (except perhaps for a few large hydrometeors that account for the radar reflectivity).

The wind discontinuity, which earlier protruded westward, continued to rotate cyclonically about the mesocyclone vertical axis and now extends southwestward ( $z = 2.8$  km). The associated shear anomaly dispersed. Accelerated rotation may have been caused by the sudden downdraft intensification within higher reflectivity regions to the north. A horizontal wind surge that accompanies the downdraft and infolds the low-level mesovortex core is displaced anticyclonically with height.

### 3.5 1603 CST: Tornado Dissipation

The downdraft within the mesocyclone core continued to strengthen while rotation of the horizontal axis apparently detached the tornado circulation from the main updraft (Fig. 11). (The more easterly tornado damage path and the now northwest-southeast orientation of the mesocyclone axis are evidence of this rotation). Exhibiting the often seen serpentine structure, the tornado weakened and was no longer visible. A shear anomaly near the intersection of the tangential wind maximum and gust front, averaging  $4 \times 10^{-2} \text{ s}^{-1}$  and extending from ground levels to 7 km, could be the remnants of the tornado.

Meanwhile, the second diffuse circulation observed at 1553 or yet another vortex center had moved or formed within the main updraft and had become the dominant rotation axis. Flow about this vertical axis now is more uniform in speed but the axis remains dislodged (west) from the core center. Generation of a new revolution axis and other morphological changes result in higher three-dimensional wind components (Fig. 12). Stronger inflow and consequent larger vertical mass flux, of course, favor additional tornadic activity, but these conditions proved only temporary. Further, the bulk of increased radial flow does not penetrate the mesocyclone core.

### 3.6 Subsequent Observations

The Harrah storm was last sampled by Doppler radar at 1611 (Figs. 13 and 14). Data show the low-level tangential wind maximum declined and the downdraft had spread to the new mesocyclone vertical axis. The shear anomaly along the gust front diminished to  $2 \times 10^{-2} \text{ s}^{-1}$  and was detectable only between 2 and 6 km elevation. Close by the mesocyclone vertical axis ( $z = 1$  to 3 km) a second anomaly ( $2 \times 10^{-2}$  to  $3 \times 10^{-2} \text{ s}^{-1}$ ) formed. Storm inflow continued to increase but remains concentrated in several locations distant from the mesocyclone core. Fig. 13 also shows a split in the principal updraft. The western component, most closely associated with the mesocyclone, declined considerably from peak values observed at 1603 while new cell growth apparently occurred farther east.

Near ground, the 40 dBZ reflectivity contour now nearly encompasses the mesocyclone core and; unlike earlier periods, reflectivity diminishes aloft. Thus, hastened by the widening downdraft within the mesovortex core, weak echo region and hook echo filling are complete. The basic radar echo shape, as determined by lower reflectivities (Fig. 1d) was conserved until at least 1800 when the storm moved beyond the radar surveillance region.

### 3.7 Summary

Mesoscale "cyclogenesis" occurred along a sheared and convergent zone between air entering both forward and rear storm quadrants. Intense rotation, first detected aloft, extended from ground through large vertical heights during the severe phase. Simultaneous development of an attendant gust front produced a surface flow configuration remarkably similar to synoptic wave cyclones.

For quantitative examination of temporal changes in the mesocyclone flow patterns and possible consequences for tornado genesis, an arbitrary radius of 3.6 km (outside the region of maximum tangential wind) was defined. The data, from the radial-height velocity distributions, are summarized in Fig. 15. Mesocyclone inflow and therefore mass flux is strong prior to tornado production and at all periods is contained primarily below 3.5 km elevation. While the surface tornado exists (1553) the level of strong outflow (divergence), heretofore above 6 km, lowers to 4 km.

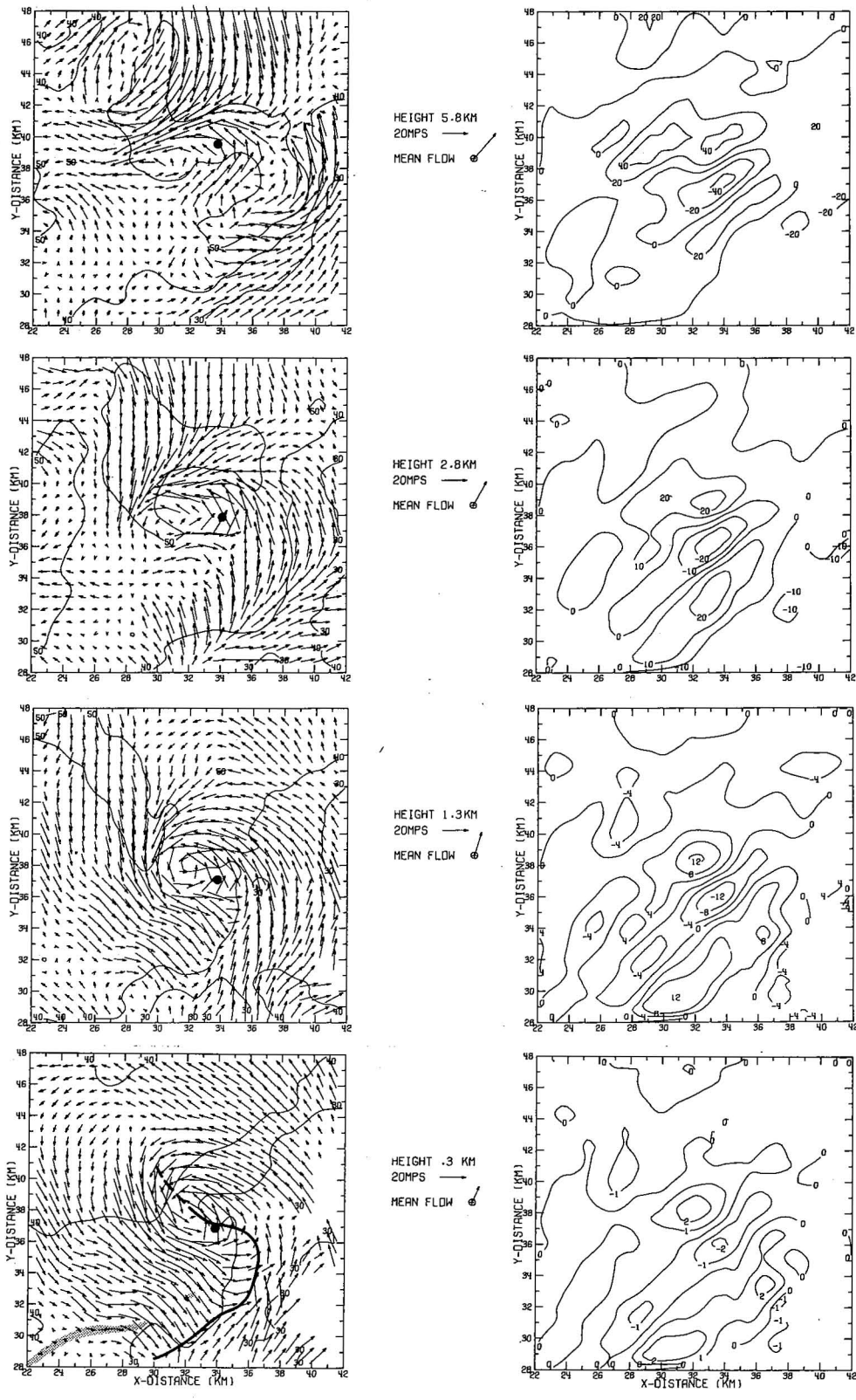


Figure 11. Horizontal wind fields, as in Fig. 7, following tornado dissipation (1603 CST).

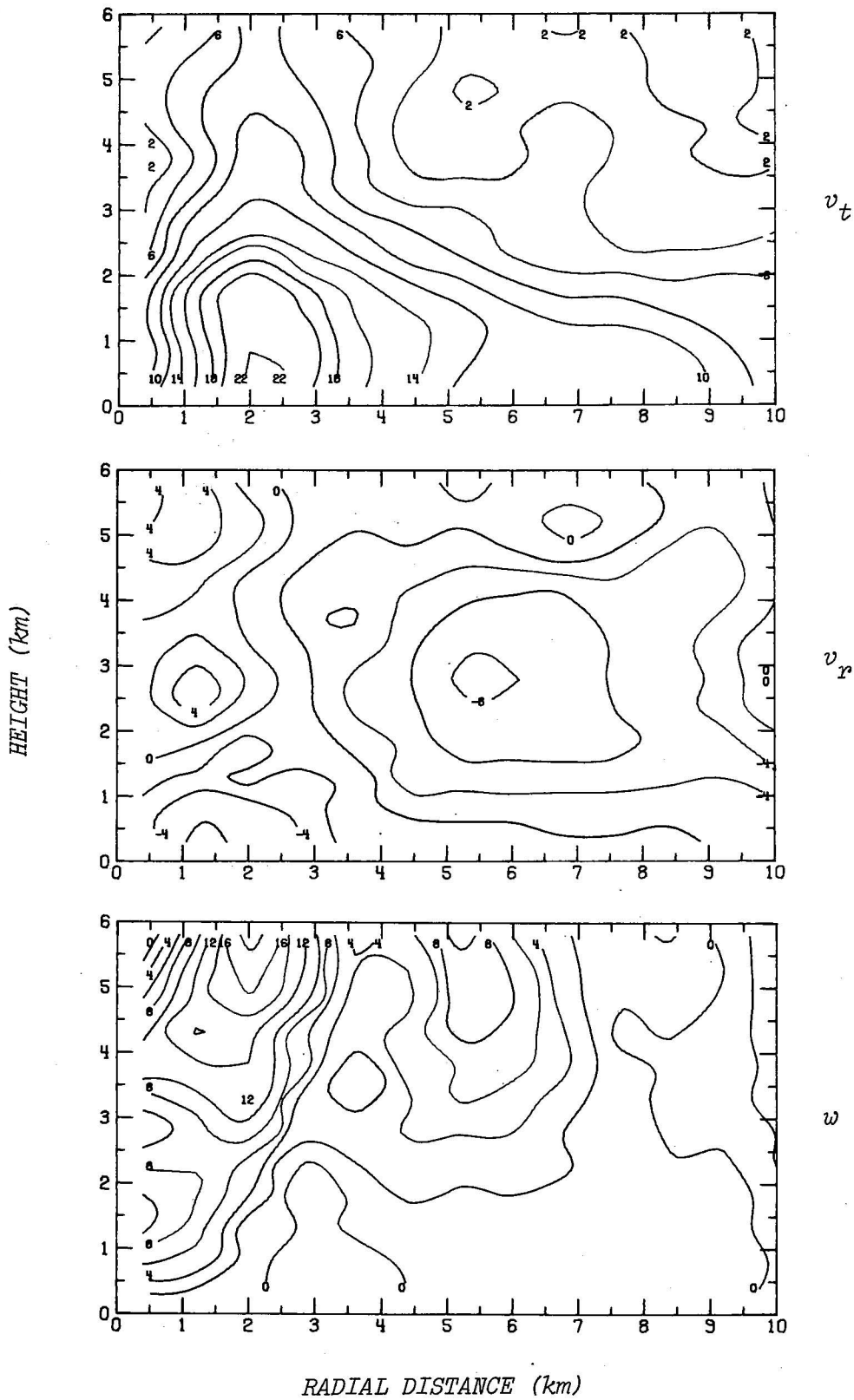


Figure 12. Radial-height distributions, as in Fig. 4, following tornado dissipation (1603 CST).

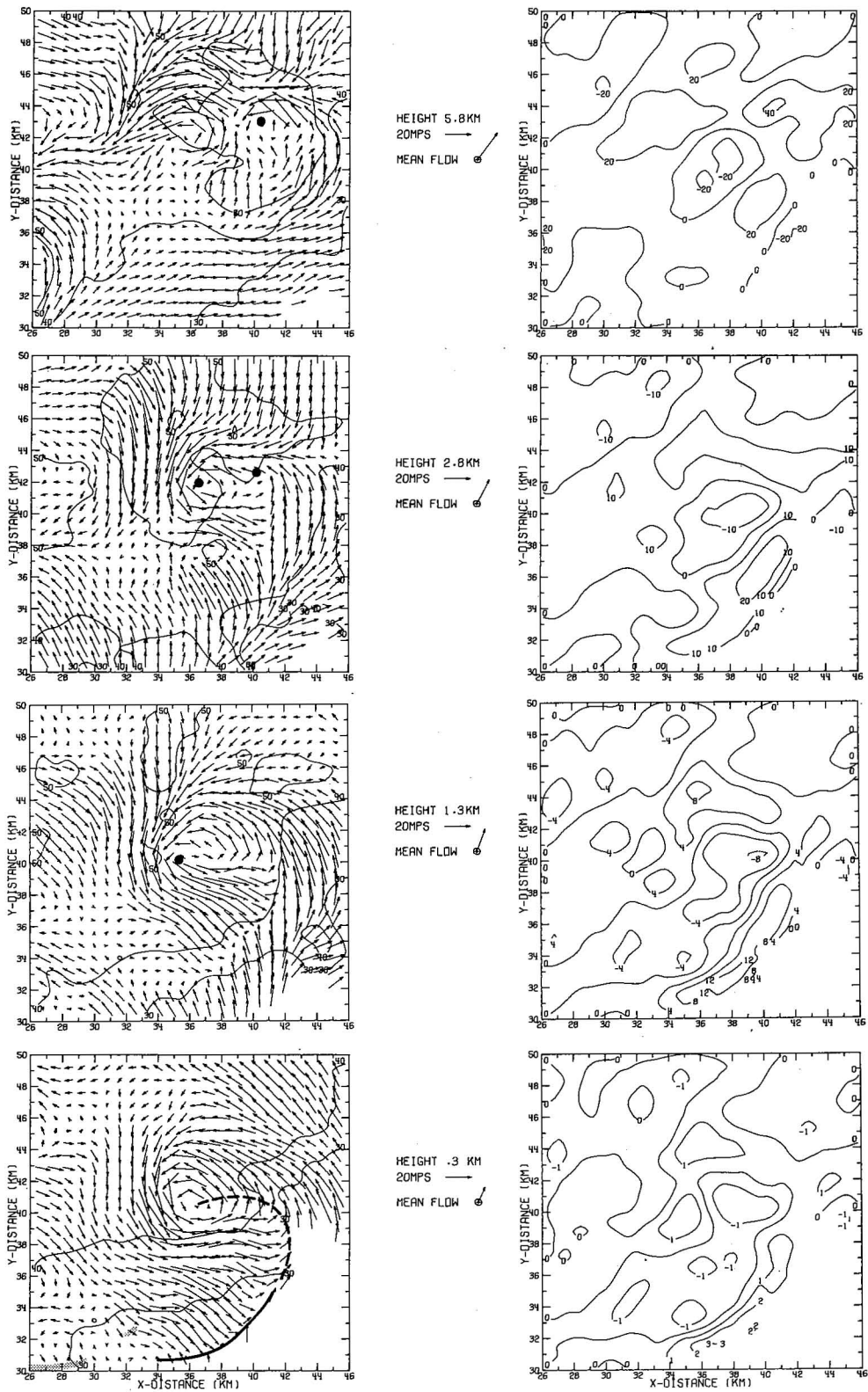


Figure 13. Horizontal wind fields, as in Fig. 7, showing continued meso-cyclone decline (1611 CST).

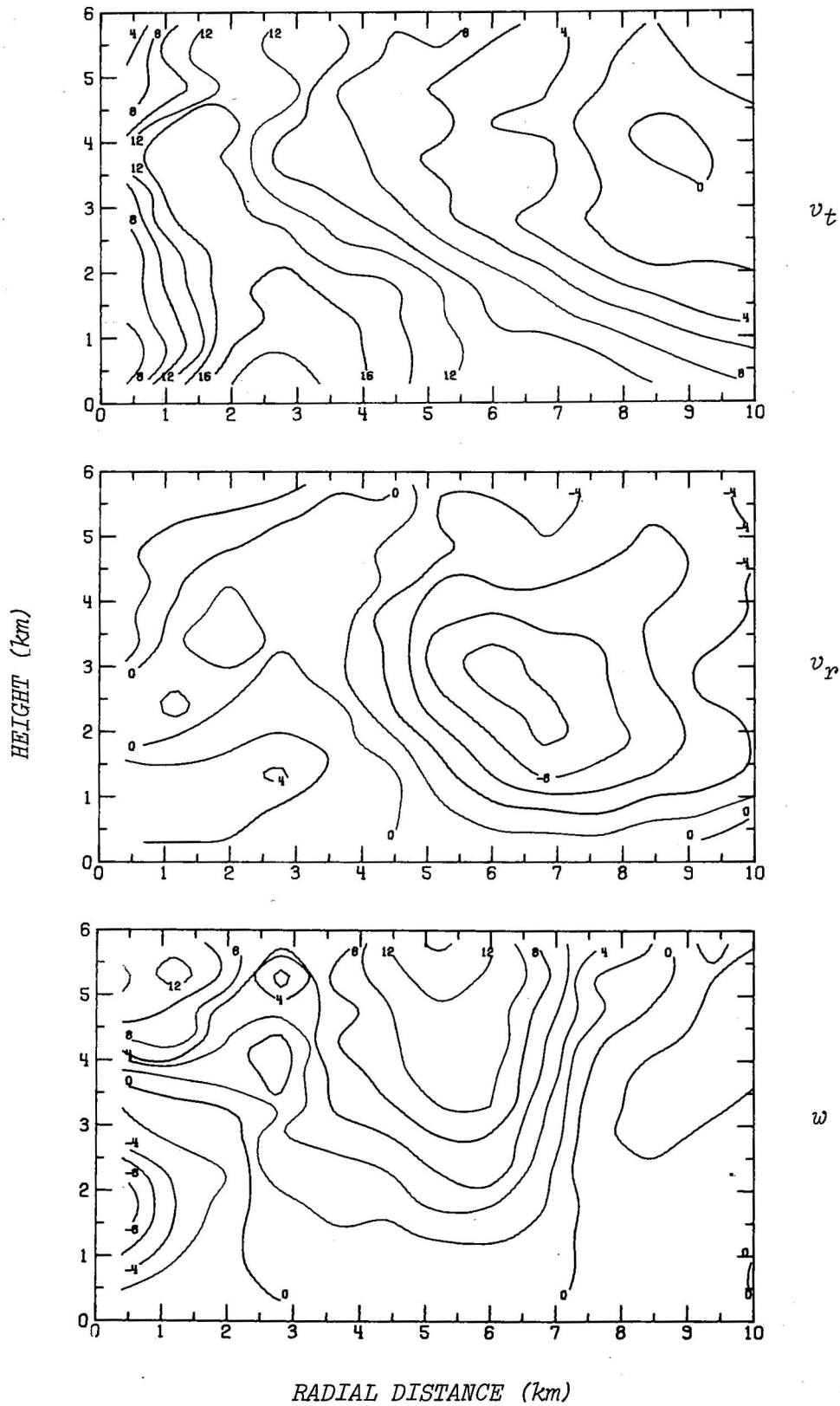


Figure 14. Radial-height velocity distributions, as in Fig. 4, showing continued mesocyclone decline (1611 CST).

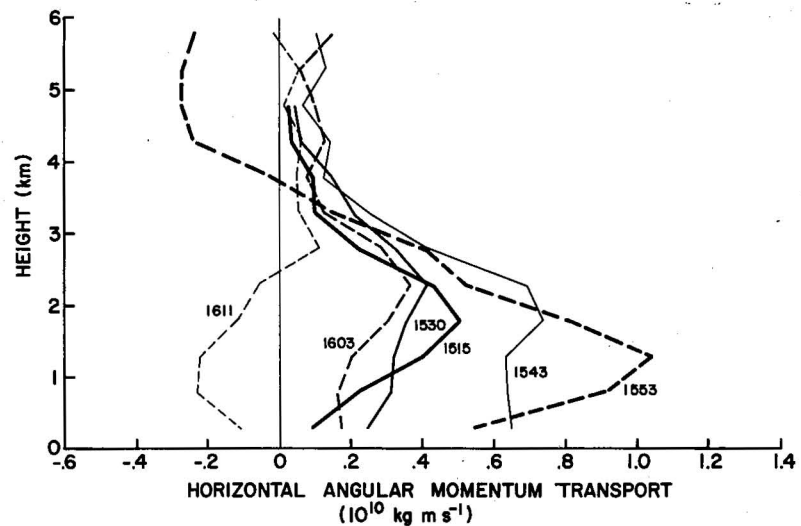
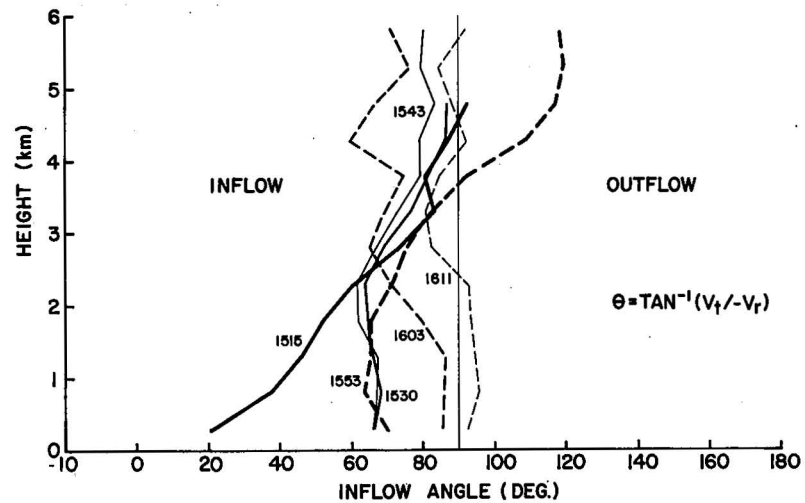
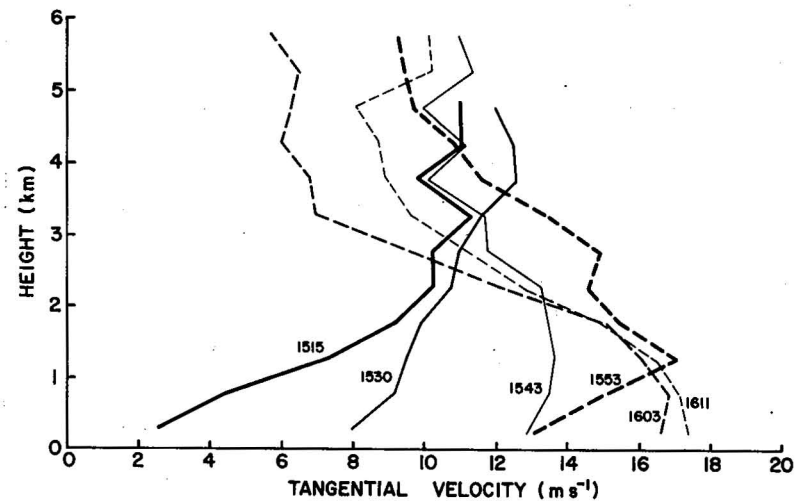
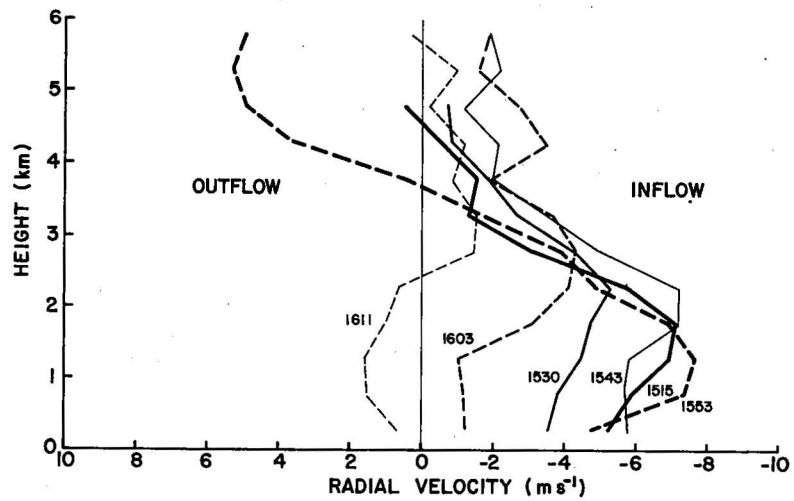


Figure 15. Mesocyclone azimuth averaged vertical profiles of radial wind, tangential wind, inflow angle, and mean horizontal angular momentum flux at 3.6 km radius.

From early mesocyclone development through tornado dissipation, there was a striking increase in swirl components at low levels and a tendency for decreasing swirl aloft. In fact, the vertical gradient of tangential wind changes sign during tornado genesis. Following dissipation of the surface tornado, low-level inflow through the mesocyclone core declines and even reverses. Hence, the data seems to substantiate the Lemon *et al.* (1975) assertion that strong swirl reduces updraft velocities for equal pressure driving forces by a "vortex valve" or choking effect. On the other hand, the greater preponderance of swirl components above 3 km height greatly reduces dilution of the mesocyclone core by intruding dry middle level air and thus may contribute to updraft maintenance.

Mean flow angular momentum flux (M), computed from

$$M = -2\pi r^2 \rho(z) \bar{v}_r \bar{v}_t, \quad (1)$$

increased conspicuously during tornado genesis and the level of maximum advection lowered while the tornado was on the ground. Both the intense mesocyclone and the embryonic tornado circulation initially were detected at or above the level of maximum flux.

Tornado genesis coincided with downdraft development within the mesocyclone core. The tornado, displaced from the core center, was located on the major horizontal mesocyclone axis in a region of strong local convergence and cyclonic shear. It's believed that initially the Harrah tornado had been attached to the principal updraft, but strong storm outflow caused rotation of the parent-vortex horizontal axis and drove the tornado from the updraft.

#### 4. FORMATION OF INTENSE VORTICES

This discussion attempts to develop a conceptual model of tornado genesis. Results of laboratory experiments are reviewed to clarify processes thought necessary for forming intense vortices.

A laboratory model thought to closely simulate updraft mesocyclones is Ward's (1972) symmetrical and mechanically driven apparatus. Ward defined a configuration ratio

$$c_r = \frac{2r_m}{h} \quad (2)$$

where  $2r_m$  is the diameter of the convective zone (updraft width) and  $h$  is the depth of the inflow layer. A single vortex forms when  $c_r = 4$  and the

inflow angle  $\theta$  [ $\equiv \tan^{-1}(v_t/-v_r)$ ] at  $r_m$  is 2 or 3°. <sup>4</sup> As the inflow angle increases, subsiding motion (vortex breakdown) begins aloft on the vertical axis and descends to the lower boundary (ground). At the axial stagnation point, a transition takes place between lower laminar flow and turbulent flow aloft within an enlarged core. When  $\theta = 30^\circ$  and  $c_r = 4$ , a vortex pair develops on opposite sides of the parent vortex. A similar result is produced for  $\theta = 75^\circ$  and  $c_r = 1.0$ . Both vortices are contained within an annulus of tangential wind and separated by divergent flow. Ward's data show strong correlation between  $r_c$  and  $\theta$  as well as between  $r_c$  and  $c_r$ . Davies-Jones (1973) re-examined Ward's data and determined  $r_c$  is primarily a function of "swirl ratio"  $S$  [ $\equiv \tan\theta (c_r/4)$ ] alone.

Similarly, the tornadic phase of the Harrah storm mesocyclone is characterized by large inflow angle, high configuration and swirl ratios, and an enlarged core (Table 1). Note also the pronounced increase in the radius of maximum inflow ( $r_m$ ). Except for 1515, the observations disclose  $r_c$  dependence upon the geometric parameters  $S$ ,  $\theta$ , and  $c_r$ .

Tornado genesis seems to involve convergent angular momentum transport within the core's favorable environment. The encircling jet-like wind annulus delineates a concentrated area of positive vertical vorticity which, for example, averages  $1.07 \times 10^{-2} \text{ s}^{-1}$  at 1543 (0.3 km height, 0.8 km grid). Coupled with the mean core convergence of  $0.54 \times 10^{-2} \text{ s}^{-1}$ , an intense tornado with  $r_c = 100 \text{ m}$  and having a circulation of  $2\pi \times 10^4 \text{ m}^2 \text{ s}^{-1}$  could be produced by convergence alone in roughly 16 min. In reality the distribution of vorticity and convergence is neither homogeneous nor isotropic.

Downward motion at the mesovortex vertical axis and bulges in the core are characteristics commonly associated with vortex breakdown. This phenomenon -- not a manifestation of instability -- rather denotes a transition between two basic axial flow types (Harvey, 1962; Benjamin, 1962). Fitzjarrold (1973) among others suggests a condition necessary for breakdown is  $w/v_t \leq 1$ ; a requirement that may have been satisfied by either the lowering plus intensification of the tangential wind annulus or the decoupling of the mesocyclone center and updraft maximum. Also, downdraft presence within the core, while high inflow is maintained, leads to concentrated updrafts (presumably) near the core radius. In advanced stages outward radial flow would be unfavorable for tornado sustenance.

Rankine and single-cell vortices of the Burgers-Rott type possess dynamic stability and resist deformation of the horizontal flow. However, Davies-Jones and Kessler (1974) point out that two-cell vortices could possess radial distributions of angular momentum which might be unstable. Moreover, they also note the vertical vorticity may be concentrated in a cylindrical sheet which, if disturbed, may become unstable and roll up into multiple vortices. In the Harrah storm several secondary eddies evolved

---

<sup>4</sup>The definition of Ward (1972) and Davies-Jones (1973) is used here. Note that an inflow angle of  $90^\circ$  ( $v_r = 0$ ) indicates purely rotational flow.

Table 1. Mesocyclone Properties

	Time CST					
	1515*	1530	1543	1553	1603	1611
h (km)	4.5	4.4	3.5	3.2	5.1	6.0
$r_m$ (km)	4.4	4.4	3.6	4.5	5.5	6.0
$c_r [=2r_m/h]$	2.0	2.0	2.1	2.7	2.2	2.0
$\theta$ (deg)	61	71	72	70	51	47
$S [= \tan \theta (c_r/4)]$	0.9	1.5	1.6	1.9	0.7	0.5
$r_c$ (km)	3.5	2.8	2.9	3.0	2.0	2.3

The average depth of the inflow layer  $h$  ( $v_r \leq -2 \text{ m s}^{-1}$ ) pertains to the region outside the mean core radius ( $r_c$ ). The convective radius ( $r_m$ ) is taken as the radial distance to the inflow maximum. Average inflow angle ( $\theta$ ), configuration ration ( $c_r$ ), and swirl ratio ( $S$ ) are all determined at  $r_m$ .

\*Data for 1515 may be unreliable.

along an elongated horizontal axis; but only the original vertical axis, displaced from the center of the mesocyclone core, became tornadic.

Downdrafts and/or related wind surges from outside the mesocyclone core could initiate a process similar to vortex breakdown and thereby alter flow properties so that instabilities will grow within the confines of the mesocyclone core. For example, Howard and Gupta (1962) determined that large horizontal gradients of vertical velocity, as observed near the tornado vortex at 1553, have a destabilizing effect on rotational flows. Recurring downdraft pulsations, rather than constant rotation of the horizontal axis, probably accounts for the periodicity noted in tornado families (Fujita, 1963; Darkow, 1971).

A combination of factors, i.e., juxtaposition of the downdrafts, proximity to the principal updraft, and presence of high shears may favor the development of tornadic vortices in the northwestern quadrant of the parent mesovortex. Near the intersection of the mesocyclone tangential wind core and the gust front a second preferred genesis region may exist. However, weaker shear and remoteness from the principal updraft suggests "gust front tornadoes" are on the average less intense and shorter lived than those that form on the opposite side of the mesocyclone core.

## 5. CONCLUSION

Tornado genesis in the Harrah storm coincided with an apparent breakdown of the parent mesovortex, i.e., the vortex increased in radius and a transition from single-cell to two-cell axial flow structure took place. During breakdown, secondary vortices appeared along an elongated horizontal axis of the mesocyclone but only the original vertical axis became tornadic. Down-draft development outside the mesocyclone core and subsequent intensification of the low-level wind flow may have initiated breakdown which then reduced vortex stability and allowed perturbation growth within the mesocyclone.

Other storms are being studied now to more firmly establish common evolutionary characteristics and the nature of instabilities that arise therein.

## 6. ACKNOWLEDGMENTS

The assistance of NSSL personnel during the preparation of this report is gratefully acknowledged. The author wishes to thank Dr. Robert Davies-Jones, Dr. Ron Alberty and Mr. Rodger Brown for their technical reviews; Ms. Helen Ardrey for providing editorial comments; and Ms. Sondra Young for typing the various drafts of the manuscript. Ms. Jennifer Moore and Mr. Charles Clark helped develop the figures. This work was partially supported under AEC Agreement #AT(49-5)-1289.

## 7. REFERENCES

- Agee, E. M., J. T. Snow and P. R. Clare, 1976: Multiple vortex features in the tornado cyclone and the occurrence of tornado families. Mon. Wea. Rev., 104, 552-563.
- Benjamin, T. B., 1962: Theory of vortex breakdown phenomenon. J. Fluid Mech. 14, 593-629.
- Brandes, E. A., 1976: Gust front evolution in severe thunderstorms: preliminary investigation with Doppler radar. Preprints Seventh Conf. on Aerospace and Aeronautical Meteorology and Symposium on Remote Sensing from Satellites, Melbourne, Fla., Amer. Meteor. Soc., Boston, Mass., 56-61.
- Brandes, E. A., 1977: Flow in severe thunderstorms observed by dual-Doppler radar. Mon. Wea. Rev., 105, 113-120.

- Browning, K. A., 1964: Airflow and precipitation trajectories within severe local storms which travel to the right of the winds. J. Atmos. Sci., 21, 634-639.
- Burgess, D. W., L. R. Lemon and R. A. Brown, 1975: Tornado characteristics revealed by Doppler radar. Geophys. Res. Lett., 2, 183-184.
- Darkow, G. L., 1971: Periodic tornado production by long-lived parent thunderstorms. Preprints Seventh Conf. Severe Local Storms, Kansas City, Mo., Amer. Meteor. Soc., Boston, Mass., 214-217.
- Davies-Jones, R. P., 1973: The dependence of core radius on swirl ratio in a tornado simulator. J. Atmos. Sci., 30, 1427-1430.
- Davies-Jones, R. P. and E. Kessler, 1974: Tornadoes Chapter 16 (552-595), Weather and Climate Modification, Editor W. N. Hess. John Wiley and Sons, New York, 842 pp.
- Fitzjarrold, D. E., 1973: A laboratory simulation of convective vortices. J. Atmos. Sci., 30, 894-902.
- Fujita, T. T., 1963: Analytical mesometeorology: a review. Meteor. Monographs, 5, No. 27, 77-125.
- Fujita, T. T., 1974: Jumbo tornado outbreak of 3 April 1974. Weatherwise, 27, 116-126.
- Harvey, J. K., 1962: Some observations of the vortex breakdown phenomenon. J. Fluid Mech., 14, 585-592.
- Heymsfield, G. M., 1976: A study of some kinematic and dynamic aspects of a severe tornadic storm. Preprints Seventeenth Conf. on Radar Meteor., Seattle, Wash., Amer. Meteor. Soc., Boston, Mass., 118-125.
- Howard, L. N. and A. S. Gupta, 1962: On the hydrodynamic and hydromagnetic stability of swirling flows. J. Fluid Mech., 14, 463-476.
- Lemon, L. R., 1976: The flanking line, a severe thunderstorm intensification source. J. Atmos. Sci., 33, 686-694.
- Lemon, L. R., D. W. Burgess and R. A. Brown, 1975: Tornado production and storm sustenance. Preprints Ninth Conf. Severe Local Storms, Norman, Okla., Amer. Meteor. Soc., Boston, Mass., 100-104.
- Marwitz, J. D., 1972: The structure and motion of severe hailstorms. Part 1: Supercell storms. J. Appl. Meteor., 11, 166-179.
- McCarthy, J., G. M. Heymsfield, and S. P. Nelson, 1974: Experiment to deduce tornado cyclone inflow characteristics using chaff and NSSL dual-Doppler radars. Bull. Amer. Meteor. Soc., 55, 1130-1131.

- Ray, P. S., R. J. Doviak, G. B. Walker, D. Sirmans, J. Carter, and B. Bumgarner, 1975: Dual-Doppler observation of a tornadic storm. J. Appl. Meteor., 14, 1521-1530.
- Ray, P. S., 1976: Vorticity and divergence fields within tornadic storms from dual-Doppler observations. J. Appl. Meteor., 15, 879-890.
- Sirmans, D. and B. Bumgarner, 1975: Numerical comparison of five mean frequency estimators. J. Appl. Meteor., 14, 991-1003.
- Ward, N. B., 1972: The exploration of certain features of tornado dynamics using a laboratory model. J. Atmos. Sci., 29, 1194-1204.

NATIONAL SEVERE STORMS LABORATORY

The NSSL Technical Memorandum, beginning with No. 28, continue the sequence established by the U. S. Weather Bureau National Severe Storms Project, Kansas City, Missouri. Numbers 1-22 were designated NSSL Reports. Numbers 23-27 were NSSL Reports, and 24-27 appeared as subseries of Weather Bureau Technical Notes. These reports are available from the National Technical Information Service, Operations Division, Springfield, Virginia 22151, for \$3.00 and a microfiche version for \$0.95. NTIS numbers are given below in parentheses.

- No. 1 National Severe Storms Project Objectives and Basic Design. Staff, NSSL. March 1961. (PB-168207)
- No. 2 The Development of Aircraft Investigations of Squall Lines from 1956-1960. B. B. Goddard. (PB-168208)
- No. 3 Instability Lines and Their Environments as Shown by Aircraft Soundings and Quasi-Horizontal Traverses. D. T. Williams. February 1962. (PB-168209)
- No. 4 On the Mechanics of the Tornado. J. R. Fulks. February 1962. (PB-168210)
- No. 5 A Summary of Field Operations and Data Collection by the National Severe Storms Project in Spring 1961. J. T. Lee. March 1962. (PB-165095)
- No. 6 Index to the NSSL Surface Network. T. Fujita. April 1962. (PB-168212)
- No. 7 The Vertical Structure of Three Dry Lines as Revealed by Aircraft Traverses. E. L. McGuire. April 1962. (PB-168213)
- No. 8 Radar Observations of a Tornado Thunderstorm in Vertical Section. Ralph J. Donaldson, Jr. April 1962. (PB-174859)
- No. 9 Dynamics of Severe Convective Storms. Chester W. Newton. July 1962. (PB-163319)
- No. 10 Some Measured Characteristics of Severe Storms Turbulence. Roy Steiner and Richard H. Rhyne. July 1962. (N62-16401)
- No. 11 A Study of the Kinematic Properties of Certain Small-Scale Systems. D. T. Williams. October 1962. (PB-168216)
- No. 12 Analysis of the Severe Weather Factor in Automatic Control of Air Route Traffic. W. Boynton Beckwith. December 1962. (PB-168217)
- No. 13 500-Kc./Sec. Sferics Studies in Severe Storms. Douglas A. Kohl and John E. Miller. April 1963. (PB-168218)
- No. 14 Field Operations of the National Severe Storms Project in Spring 1962. L. D. Sanders. May 1963. (PB-168219)
- No. 15 Penetrations of Thunderstorms by an Aircraft Flying at Supersonic Speeds. G. P. Roys. Radar Photographs and Gust Loads in Three Storms of 1961 Rough Rider. Paul W. J. Schumacher. May 1963. (PB-168220)
- No. 16 Analysis of Selected Aircraft Data from NSSL Operations, 1962. T. Fujita. May 1963. (PB-168221)
- No. 17 Analysis of Methods for Small-Scale Surface Network Data. D. T. Williams. August 1963. (PB-168222)
- No. 18 The Thunderstorm Wake of May 4, 1961. D. T. Williams. August 1963. (PB-168223)
- No. 19 Measurements by Aircraft of Condensed Water in Great Plains Thunderstorms. George P. Roys and Edwin Kessler. July 1966. (PB-173048)
- No. 20 Field Operations of the National Severe Storms Project in Spring 1963. J. T. Lee, L. D. Sanders, and D. T. Williams. January 1964. (PB-168224)
- No. 21 On the Motion and Predictability of Convective Systems as Related to the Upper Winds in a Case of Small Turning of Wind with Height. James C. Fankhauser. January 1964. (PB-168225)
- No. 22 Movement and Development Patterns of Convective Storms and Forecasting the Probability of Storm Passage at a Given Location. Chester W. Newton and James C. Fankhauser. January 1964. (PB-168226)
- No. 23 Purposes and Programs of the National Severe Storms Laboratory, Norman, Oklahoma. Edwin Kessler. December 1964. (PB-166675)

- No. 24 Papers on Weather Radar, Atmospheric Turbulence, Sferics, and Data Processing. August 1965. (AD-621586)
- No. 25 A Comparison of Kinematically Computed Precipitation with Observed Convective Rainfall. James C. Fankhauser. September 1965. (PB-168445)
- No. 26 Probing Air Motion by Doppler Analysis of Radar Clear Air Returns. Roger M. Lhermitte. May 1966. (PB-170636)
- No. 27 Statistical Properties of Radar Echo Patterns and the Radar Echo Process. Larry Armijo. May 1966. The Role of the Kutta-Joukowski Force in Cloud Systems with Circulation. J. L. Goldman. May 1966. (PB-170756)
- No. 28 Movement and Predictability of Radar Echoes. James Warren Wilson. November 1966. (PB-173972)
- No. 29 Notes on Thunderstorm Motions, Heights, and Circulations. T. W. Harrold, W. T. Roach, and Kenneth E. Wilk. November 1966. (AD-644899)
- No. 30 Turbulence in Clear Air Near Thunderstorms. Anne Burns, Terence W. Harrold, Jack Burnham, and Clifford S. Spavins. December 1966. (PB-173992)
- No. 31 Study of a Left-Moving Thunderstorm of 23 April 1964. George R. Hammond. April 1967. (PB-174681)
- No. 32 Thunderstorm Circulations and Turbulence from Aircraft and Radar Data. James C. Fankhauser and J. T. Lee. April 1967. (PB-174860)
- No. 33 On the Continuity of Water Substance. Edwin Kessler. April 1967. (PB-175840)
- No. 34 Note on the Probing Balloon Motion by Doppler Radar. Roger M. Lhermitte. July 1967. (PB-175930)
- No. 35 A Theory for the Determination of Wind and Precipitation Velocities with Doppler Radars. Larry Armijo. August 1967. (PB-176376)
- No. 36 A Preliminary Evaluation of the F-100 Rough Rider Turbulence Measurement System. U. O. Lappe. October 1967. (PB-177037)
- No. 37 Preliminary Quantitative Analysis of Airborne Weather Radar. Lester P. Merritt. December 1967. (PB-177188)
- No. 38 On the Source of Thunderstorm Rotation. Stanley L. Barnes. March 1968. (PB-178990)
- No. 39 Thunderstorm - Environment Interactions Revealed by Chaff Trajectories in the Mid-Troposphere. James C. Fankhauser. June 1968. (PB-179659)
- No. 40 Objective Detection and Correction of Errors in Radiosonde Data. Rex L. Inman. June 1968. (PB-180284)
- No. 41 Structure and Movement of the Severe Thunderstorms of 3 April 1964 as Revealed from Radar and Surface Mesonetwork Data Analysis. Jess Charba and Yoshikazu Sasaki. October 1968. (PB-183310)
- No. 42 A Rainfall Rate Sensor. Brian E. Morgan. November 1968. (PB-183979)
- No. 43 Detection and Presentation of Severe Thunderstorms by Airborne and Ground-Based Radars: A Comparative Study. Kenneth E. Wilk, John K. Carter, and J. T. Dooley. February 1969. (PB-183572)
- No. 44 A Study of a Severe Local Storm of 16 April 1967. George Thomas Haglund. May 1969. (PB-184970)
- No. 45 On the Relationship Between Horizontal Moisture Convergence and Convective Cloud Formation. Horace R. Hudson. March 1970. (PB-191720)
- No. 46 Severe Thunderstorm Radar Echo Motion and Related Weather Events Hazardous to Aviation Operations. Peter A. Barclay and Kenneth E. Wilk. June 1970. (PB-192498)
- No. 47 Evaluation of Roughness Lengths at the NSSL-WKY Meteorological Tower. Leslie D. Sanders and Allen H. Weber. August 1970. (PB-194587)
- No. 48 Behavior of Winds in the Lowest 1500 ft in Central Oklahoma: June 1966-May 1967. Kenneth C. Crawford and Horace R. Hudson. August 1970.
- No. 49 Tornado Incidence Maps. Arnold Court. August 1970. (COM-71-00019)
- No. 50 The Meteorologically Instrumented WKY-TV Tower Facility. John K. Carter. September 1970. (COM-71-00108)

- No. 51 Papers on Operational Objective Analysis Schemes at the National Severe Storms Forecast Center. Rex L. Inman. November 1970. (COM-71-00136)
- No. 52 The Exploration of Certain Features of Tornado Dynamics Using a Laboratory Model. Neil B. Ward. November 1970. (COM-71-00139)
- No. 53 Rawinsonde Observation and Processing Techniques at the National Severe Storms Laboratory. Stanley L. Barnes, James H. Henderson, and Robert J. Ketchum. April 1971. (COM-71-00707)
- No. 54 Model of Precipitation and Vertical Air Currents. Edwin Kessler and William C. Bumgarner. June 1971. (COM-71-00911)
- No. 55 The NSSL Surface Network and Observations of Hazardous Wind Gusts. Operations Staff. June 1971. (COM-71-00910)
- No. 56 Pilot Chaff Project at the National Severe Storms Laboratory. Edward A. Jessup. November 1971. (COM-72-10106)
- No. 57 Numerical Simulation of Convective Vortices. Robert P. Davies-Jones and Glenn T. Vickers. November 1971. (COM-72-10269).
- No. 58 The Thermal Structure of the Lowest Half Kilometer in Central Oklahoma: December 9, 1966-May 31, 1967. R. Craig Goff and Horace R. Hudson. July 1972. (COM-72-11281)
- No. 59 Cloud-to-Ground Lightning Versus Radar Reflectivity in Oklahoma Thunderstorms. Gilbert D. Kinzer. September 1972. (COM-73-10050)
- No. 60 Simulated Real Time Displays of Velocity Fields by Doppler Radar. L. D. Hennington and G. B. Walker. November 1972. (COM-73-10515)
- No. 61 Gravity Current Model Applied to Analysis of Squall-Line Gust Front. Jess Charba. November 1972. (COM-73-10410)
- No. 62 Mesoscale Objective Map Analysis Using Weighted Time-Series Observations. Stanley L. Barnes. March 1973. (COM-73-10781)
- No. 63 Observations of Severe Storms on 26 and 28 April 1971. Charles L. Vitek. April 1973. (COM-73-11200)
- No. 64 Meteorological Radar Signal Intensity Estimation. Dale Sirmans and R. J. Doviak. September 1973. (COM-73-11923/2AS)
- No. 65 Radiosonde Altitude Measurement Using Double Radiotheodolite Techniques. Stephan P. Nelson. September 1973. (COM-73-11934/9AS)
- No. 66 The Motion and Morphology of the Dryline. Joseph T. Schaefer. September 1973. (COM-74-10043)
- No. 67 Radar Rainfall Pattern Optimizing Technique. Edward A. Brandes. March 1974. (COM-74-10906/AS)
- No. 68 The NSSL/WKY-TV Tower Data Collection Program: April-July 1972. R. Craig Goff and W. David Zittel. May 1974. (COM-74-11334/AS)
- No. 69 Papers on Oklahoma Thunderstorms, April 29-30, 1970. Stanley L. Barnes, Editor. May 1974. (COM-74-11474/AS)
- No. 70 Life Cycle of Florida Key's Waterspouts. Joseph H. Golden. June 1974. (COM-74-11477/AS)
- No. 71 Interaction of Two Convective Scales Within a Severe Thunderstorm: A Case Study and Thunderstorm Wake Vortex Structure and Aerodynamic Origin. Leslie R. Lemon. June 1974. (COM-74-11642/AS)
- No. 72 Updraft Properties Deduced from Rawinsoundings. Robert P. Davies-Jones and James H. Henderson. October 1974. (COM-75-10193/AS)
- No. 73 Severe Rainstorm at Enid, Oklahoma - October 10, 1973. L. P. Merritt, K. E. Wilk, and M. L. Weible. November 1974. (COM-75-10583/AS)
- No. 74 Mesonet Array: Its Effect on Thunderstorm Flow Resolution. Stanley L. Barnes. October 1974. (COM-75-10248/AS)
- No. 75 Thunderstorm-Outflow Kinematics and Dynamics. R. Craig Goff. December 1975. (PB-250808/AS)
- No. 76 An Analysis of Weather Spectra Variance in a Tornadic Storm. Philippe Waldeufel. May 1976. (PB-258456/AS)
- No. 77 Normalized Indices of Destruction and Deaths by Tornadoes. Edwin Kessler and J. T. Lee. June 1976. (PB-260923/AS)

- No. 78 Objectives and Accomplishments of the NSSL 1975 Spring Program. K. Wilk, K. Gray, C. Clark, D. Sirmans, J. T. Dooley, J. Carter, and W. Bumgarner. July 1976. (PB-263813/AS)
- No. 79 Subsynoptic Scale Dynamics As Revealed By The Use Of Filtered Surface Data. Charles A. Doswell III. December 1976. (PB-265433/AS)
- No. 80 The Union City, Oklahoma Tornado of 24 May 1973. Rodger A. Brown, Editor. December 1976.

